Physics – Uspekhi **47** (9) 887 – 905 (2004)

REVIEWS OF TOPICAL PROBLEMS PACS numbers: 41.75.Fr, **51.50.+v**, 52.80.Dy

The electron runaway mechanism in dense gases and the production of high-power subnanosecond electron beams

V F Tarasenko, S I Yakovlenko

DOI: 10.1070/PU2004v047n09ABEH001790

Contents

Abstract. New insight is provided into how runaway electrons are generated in gases. It is shown that the Townsend mechanism of electron multiplication works even for strong fields, when the ionization friction of electrons can be neglected. The nonlocal electron runaway criterion proposed in the work determines the critical voltage – *pd* relationship as a two-valued function universal for a given gas (*p* being the gas pressure, and *d* the electrode spacing). This relationship exhibits an additional upper branch as contrasted to the familiar Paschen's curves and divides the discharge gap into two regions: one where electrons multiply effectively, and the other which they leave without having enough time to multiply. Experiments on the production of electron beams with subnanosecond pulse duration and an amplitude of tens to hundreds of amperes at atmospheric pressure in various gases are addressed, and the creation of a nanosecond volume discharge with the high density of excitation power and without preionization of the gap by a supplementary source is discussed.

V F Tarasenko Institute of High Current Electronics,
Siberian Branch of the Russian Academy of Sciences,
Akademicheskiĭ prosp. 2/3, 634055 Tomsk, Russian Federation
Tel. (7-3822) 49 16 85. Fax (7-3822) 49 24 10
E-mail: vtf@loi.hcei.tsc.ru
S I Yakovlenko A M Prokhorov General Physics Institute,
Russian Academy of Sciences,
ul. Vavilova 38, 119942 Moscow, Russian Federation
Tel. (7-095) 132 82 80, (7-095) 132 81 45
Fax (7-095) 135 79 22
E-mail: syakov@kapella.gpi.ru, s.yakov@g23.relcom.ru

Received 3 December 2003, revised 14 April 2004
Uspekhi Fizicheskikh Nauk **174** (9) 953 – 971 (2004)
Translated by E Yankovsky; edited by A Radzig

1. Introduction

In the present review, we discuss three aspects of the physics of discharges at pressures on the order of atmospheric pressure, which are related to the production of high-power subnanosecond electron beams. First, we give a review of works that have formed the basis for the new understanding of the mechanism of production of a beam of runaway electrons in gases (Section 2). Second, we present the results of experiments on the production of electron beams of subnanosecond duration with a record amplitude of the current in gas-filled atmospheric-pressure diodes (Section 3). Third, we analyze some properties of volume discharges of nanosecond duration, properties that have helped produce such powerful beams (Section 4).

As is well known, the runaway of electrons (the whistler mode) occurs in fully ionized plasma placed in a strong electric field, when the majority of electrons acquire on their mean free path more energy from the field than they lose in elastic collisions, with the result that the electrons are continuously accelerated. The phenomenon of runaway of electrons in plasma was predicted long ago by Giovanelly [1]; the numerical calculations of this effect were done by Dreicer [2] and Kulsrud et al. [3], and an analytical investigation for the case of weak fields was carried out by Gurevich [4]. The phenomenon has proved important in the diagnostics and energy balance of impurities in tokamak plasmas [5].

Runaway of electrons can also be observed in gases (see the references cited in the review [6] and in the monographs [7, 8]). It triggers what is known as open discharges in gases of moderate density [9 – 13] (such discharges are used, among other things, to pump lasers [9, 14, 15]). It is customary to assume that runaway of electrons in a gas is

described in approximately the same way as in a fully ionized plasma, i.e., the assumption is that runaway of electrons sets in when the force with which the electric field acts on an electron exceeds the decelerating force [6–8]. However, computer simulations and analytical treatment suggest that most electrons in a gas occupying a fairly large volume are not continuously accelerated [16–19]. No matter how high the electric field strength is, at certain distances from the cathode the Townsend ionization mode sets in for the vast majority of electrons, and this mode is determined by two factors. First, the number of ionization acts grows exponentially with the distance from the cathode. Second, the mean velocity and energy of the electrons do not depend on this distance.

The common approach [6–8] leads to a local criterion for the electric field strength that determines the condition in which, as is ordinarily assumed, many runaway electrons appear. The criterion is that the electric field strength must exceed the value at which the energy that an electron acquires on the mean free path is balanced by the maximum energy loss through ionization of the gas.

In Section 2 we discuss the reasons why the ordinary approach cannot be applied to the majority of electrons in conditions of electron multiplication, with the result that the local criterion cannot be used for describing the conditions of production of a powerful beam of runaway electrons in a gas. We propose a nonlocal electron runaway criterion in the form of a universal two-valued dependence for the 'critical' voltage U_{cr} on pd for the given gas, where p is the gas pressure, and d is the distance between the flat electrodes. These curves separate the region of effective electron multiplication from the region where the electrons leave the discharge gap before they have any time to multiply. We present the results of simulation of the Townsend coefficients for helium, neon, xenon, nitrogen, and sulfur hexafluoride.

The study covering the mechanism of runaway electron production in a gas has become especially important in connection with the problem of generating electron beams of subnanosecond duration with record current amplitudes (~ 70 A in air, and ~ 200 A in helium [20–25]) at atmospheric pressure. In Section 3 we discuss the results of experiments on generating high-power subnanosecond electron beams at atmospheric pressure and examine some aspects of the mechanism of electron-beam production when the nonlocal electron runaway criterion is met. It has been found that an electron beam is produced at the stage when the plasma being formed at the cathode closes in on the anode, as if the plasma brings the cathode closer to the anode, which leads to a condition where the nonlocal electron runaway criterion is met. Here, the voltage U and the parameter pd are to be found near the upper branches of the curves characterizing the criterion of electron escape without multiplication.

The stage of formation of a plasma cathode approaching the anode is discussed in Section 4. We show that a self-sustained nanosecond discharge in a dense gas is possible when the gap voltage is at its maximum at the quasi-steady stage of the discharge. In this case, the input power density may exceed 400 MW cm^{-3}. We also examine the role of preionization by fast electrons emitted by a plasma spike at the cathode and the electron multiplication wave traveling from the anode to the cathode.

2. Electron multiplication and runaway electrons

2.1 Local electron runaway criterion

2.1.1 The traditional approach. Let us briefly discuss the main aspects of deriving the local electron runaway criterion (a detailed derivation can be found, e.g., in Refs [6, p. 53; 7, p. 71; 8, p. 74]). It is assumed that in the stable flow of electrons from the cathode to the anode their distribution is close to monoenergetic [8]. For the energy ε of an electron in an electric field of strength E, the following energy balance equation is used in the simplest case:

$$\frac{d\varepsilon}{dx} = eE - F(\varepsilon), \tag{1}$$

where x is the distance measured from the cathode, and $F(\varepsilon)$ is the force of friction caused by the collisions of the electron with the gas atoms. The friction force in the nonrelativistic case is often represented in the simple form based on the Bethe approximation [7]:

$$F(\varepsilon) = \frac{2\pi e^4 ZN}{\varepsilon} \ln\left(\frac{2\varepsilon}{I}\right). \tag{2}$$

Here, Z is the number of electrons in the atom or molecule of the neutral gas, N is the particle number density in the neutral gas, and I is the mean inelastic energy loss. Despite the rough nature of approximation (2), it gives birth to (and so do more precise calculations) the maximum in the dependence of the friction force on the electron energy, $F_{max} = F(\varepsilon_{max})$ (Fig. 1), attained at $\varepsilon_{max} = 2.72\, I/2$. For helium, $I = 44$ eV and $\varepsilon_{max} = 2.72\, I/2 = 60$ eV; a more exact calculation yields $\varepsilon_{max} \approx 100$ eV. For nitrogen, $I = 80$ eV and $\varepsilon_{max} = 2.72\, I/2 = 109$ eV, whereas a more exact calculation produces $\varepsilon_{max} \approx 103$ eV.

According to the traditional approach [6–8], the condition for a runaway electron to appear in a gas is the requirement that electric field strength be high, $E > E_{cr1}$, where the critical field strength E_{cr1} is determined by the maximum value of the decelerating force, $E_{cr1} = F_{max}/e$. For instance, when expression (2) is used for the critical field, we have [7]

$$E_{cr1} = \frac{4\pi e^3 ZN}{2.72\, I} \quad \text{or} \quad \frac{E_{cr1}}{p} = 3 \times 10^3 \frac{Z}{I}\ [\mathrm{V\,cm^{-1}\,Torr^{-1}}], \tag{3}$$

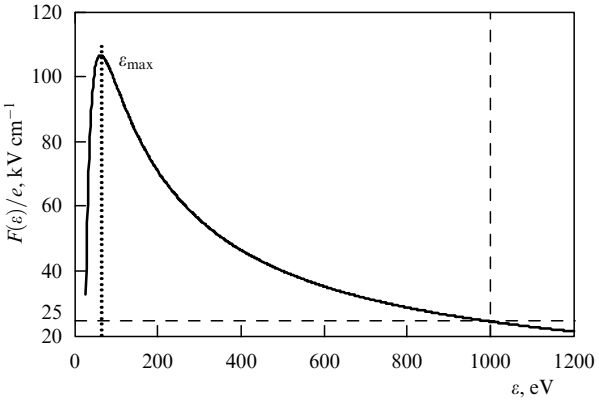

Figure 1. Dependence of the ionization-induced decelerating force per electron charge on the electron energy for helium at atmospheric pressure.

where p is the gas pressure at 300 K, and I is measured in electron-volts. For example, in helium $E_{cr1}/p \approx 140$ V cm^{-1} Torr^{-1}, while for nitrogen $E_{cr1}/p \approx 590$ V cm^{-1} Torr^{-1}.

The criterion $E > E_{cr1}$ is local in the sense that the critical field E_{cr1} is determined solely by the properties of the neutral particles and the gas density at the given point in space.

Following are some simple ideas explaining why the whistler mode, i.e., continuous acceleration of the majority of electrons in gases, is not actually realized even when $E > E_{cr1}$ if the distance to the cathode is sufficiently large.

2.1.2 Limitation on the mean energy due to electron multiplication. An important fact must be taken into account in this case. Even when $E > E_{cr1}$, the mean electron energy will not increase without limit with a rise in x, even if we completely ignore the friction force. The point is that the reasoning in Section 2.1.1 does not take into consideration an important fact, namely, the multiplication of electrons. Note that although the electron multiplication is a well-known fact [6–8], the importance of the effect of this process on the electron runaway criterion is usually overlooked.

To determine the mean electron energy ε^*, we must turn not to equation (1) but to an equation that allows for a change in the number of electrons. In the simplest case, on the level of approximation (1), the law of conservation of energy can be written in the form

$$\frac{d(N_e\varepsilon^*)}{dx} = eEN_e - F(\varepsilon^*)N_e\,, \tag{4}$$

where $N_e(x)$ is the electron number density at point x. Since $dN_e/dx = \alpha_i N_e$, where α_i is the Townsend electron multiplication coefficient, equation (4) yields the following equation for the mean electron energy ε^*:

$$\frac{d\varepsilon^*}{dx} = eE - F(\varepsilon^*) - \alpha_i\varepsilon^*\,. \tag{5}$$

In contrast to Eqn (1), equation (5) contains a negative term $\alpha_i\varepsilon^*$ on the right-hand side, which describes the 'smearing' of the energy acquired by the electrons from the electric field onto all electrons, including secondary ones. Hence, even if we ignore electron deceleration in the gaseous medium [i.e., $F(\varepsilon) = 0$], the mean electron energy is limited: $\varepsilon^* < \varepsilon^*_{max} = eE/\alpha_i$. Therefore, it is impossible to think that Eqn (1) constitutes an equation for the mean electron energy and that the electron distribution is monoenergetic.

When for some reason ionization is absent ($\alpha_i = 0$), the traditional approach based on equation (1) is valid. For instance, electron deceleration in a fully ionized plasma is caused by elastic Coulomb collisions, and a detailed study of this problem yields an expression for the critical field, $E_{cr1} = 4\pi e^3 \Lambda N/T$ (e.g., see Ref. [3]), which qualitatively is similar to formula (3). Here, Λ is what is known as the Coulomb logarithm, N is the number density of the charged particles, and T is the plasma temperature.

Of course, equation (5) represents an approximate one, just as Eqn (1) is. In particular, it is one-dimensional and does not account for the fact that secondary electrons also have some energy. In contrast to the traditional approach, however, equation (5) clearly illustrates that in the event of exponential electron multiplication the mean energy of the electrons (and hence the mean velocity) cannot increase progressively with x. At a certain distance (see Section 2.3), we can put $d\varepsilon^*/dx = 0$, and $\varepsilon^* = \text{const}$.

The aforesaid implies that for the majority of electrons the Townsend multiplication mode (in which the fraction of continuously accelerated electrons is small) is implemented even in high fields $E > E_{cr1}$, when, according to the common viewpoint, all the electrons are accelerated steadily. Of course, some of the fast electrons are indeed accelerated at all times. Moreover, such electrons can play an important role in the gas preionization (see Section 4.2). However, at a certain distance from the cathode the fraction of these continuously accelerated electrons is small compared to the overall number of electrons, since the mean electron energy ceases to increase over this distance. In this connection, we turn to the results of numerical simulation.

2.2 Electron multiplication

2.2.1 The model. To confirm the assumption that the Townsend coefficient does not lose its meaning even when $E > E_{cr1}$, mathematical modeling of electron multiplication and runaway of electrons have been carried out for He [16], Ne,[1] Xe [17], N_2 [19], and SF_6 [18] on the basis of a modification of the particle method [26]. The electrons produced at the cathode had randomly directed velocities and initial energies distributed according to the Poisson law with the mean value $\varepsilon_0 = 0.2$ eV. Multiple and stepwise ionization, the electron–electron interaction, and the screening of the external electric field were not taken into account. The equations of motion of all the electrons were solved on a mesh with small temporal steps, while elastic and inelastic collisions were modelled with probabilities determined by the cross sections of the elementary processes.

Below, we present the results for flat electrodes separated by a distance d with a voltage U applied to them. Although plasma inhomogeneity is essential in real experiments (see Sections 3 and 4), the two-dimensional model makes it possible to expose many important aspects of the physics of gas breakdown (the manner for applying the method to the case of coaxial cylinders is described in Ref. [26]).

For helium, the excitation of the states $2\,^3S$, $2\,^1S$, $2\,^3P$, and $2\,^1P$ was taken into account, and for xenon the excitation of the state $5p^56s$ ($J = 1$) with the energy $E = 8.44$ eV. The results given in Refs [27–29] were used in the case of helium, and those in Refs [26, 30, 31] in the case of xenon. The electron–nitrogen-molecule scattering cross section was determined on the basis of the data listed in Refs [32–43]. The excitation of the 10 lowest electronic states of the nitrogen molecule and the 8 lowest vibrational states was taken into account. In modeling the processes in SF_6, the data on the cross sections and energy depositions were taken from Refs [44–46].

2.2.2 The Townsend ionization mode. The results of calculations described in Refs [16–19] show that for all values of the reduced field strength and large enough distances d between the electrodes, the Townsend ionization mode is truly present and runaway electrons are practically absent. That the ionization mode is indeed the Townsend one is confirmed by the fact that as the distance x from the cathode is increased, the number of acts of excitation and electron production increases exponentially for all time beginning from some values of x. In this case, the mean electron energy ε^* and the mean projection of electron velocity on the x-axis do not

[1] The calculations for neon were done by A N Tkachev, A A Fedenev, and S I Yakovlenko.

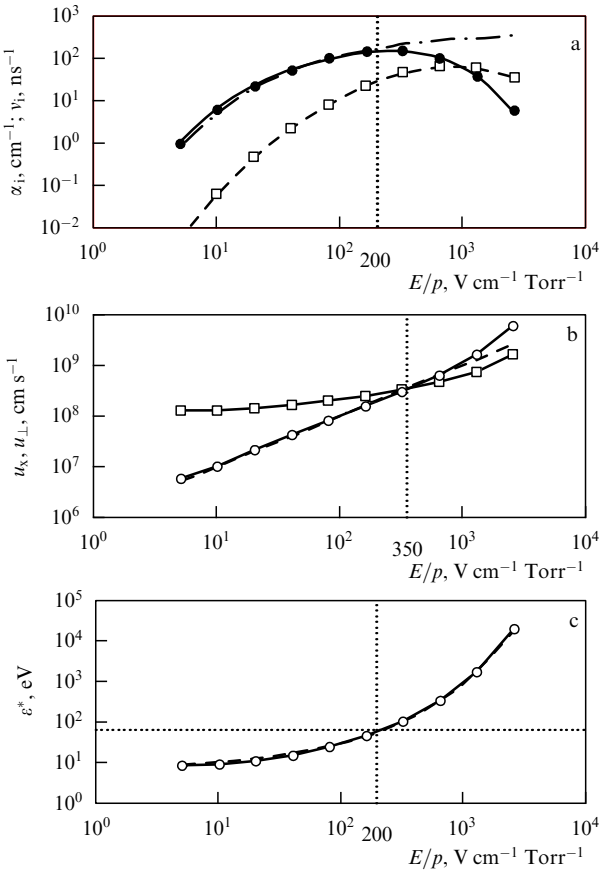

Figure 2. Dependence of the ionization and drift characteristics on the reduced field strength E/p in helium. The points were obtained for different values of electric field strength. Everywhere, if not stated otherwise, $N = 3.22 \times 10^{18}$ cm^{-3} ($p = 100$ Torr). (a) Pressure-normalized values of the Townsend coefficient α_i/p (black circles) and of the ionization rate ν_i/p (open squares). The heavy solid curve corresponds to approximation (7), and the dot-and-dash curve to approximation (6). (b) Mean projection u_x (open circles) of the electron velocity on the x-axis directed along the electric field, and the mean absolute value of the velocity $u_\perp$ (open squares) in the plane perpendicular to the x-axis. The dashed straight line corresponds to the linear dependence $u_x = 10^6(E/p)$ cm s^{-1}, where the unit of measurement of E/p is 1 V cm^{-1} Torr^{-1}. (c) Mean electron energy (obtained by simulation for different values of electric field strength). The dashed curve corresponds to the dependence $\varepsilon^* = 5.5 \exp\left(\sqrt{E/(40p)}\right)$ eV, where the unit of measurement of E/p is 1 V cm^{-1} Torr^{-1}.

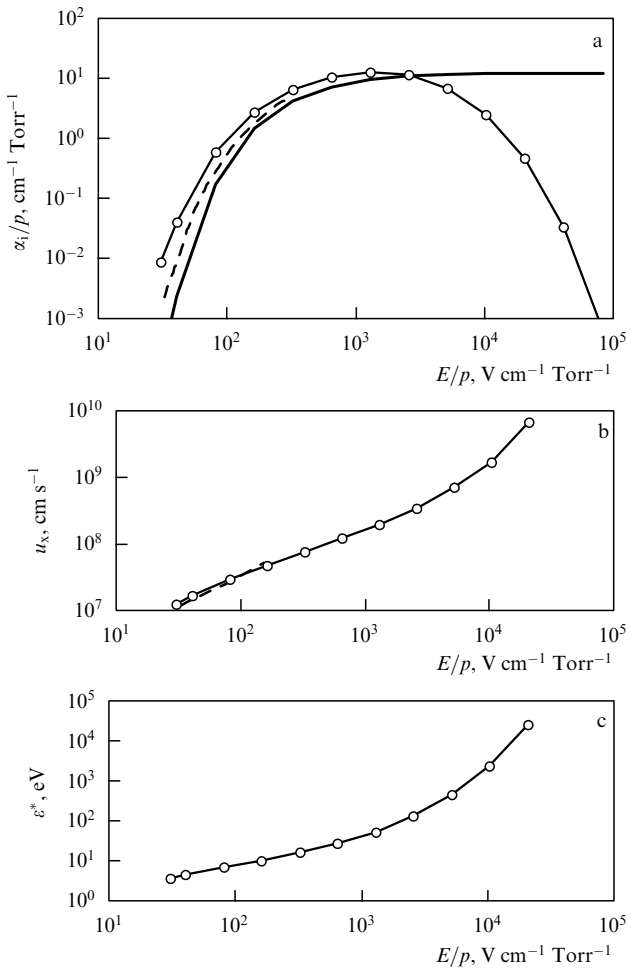

Figure 3. Dependence of the ionization and drift characteristics on the reduced field strength E/p for nitrogen N_2. The points were obtained for different electric field strengths at $p = 100$ Torr ($N = 3.22 \times 10^{18}$ cm^{-3}). (a) Pressure-normalized values of the Townsend coefficient α_i/p (open circles) obtained as a result of simulation for different values of the field strength. The heavy solid curve corresponds to approximation (6), and the dashed curve to the results of simulation [27]. (b) Mean projection u_x (open circles) of the electron velocity on the x-axis directed along the electric field, with the dashed curve corresponding to the results of simulation [27]. (c) Mean electron energy.

depend on x at sufficiently large distances from the cathode. The maximum of the distribution function of the electrons that reach the anode lies in the region of low mean electron energies, $\varepsilon^* \ll eU$. As noted earlier, all these indications of a Townsend ionization mode occur both for $E/p \leqslant E_{cr1}/p$ and for $E/p > E_{cr1}/p$. What is important is that the distance d between the electrodes be large (see below and Ref. [16]).

The calculations that were performed for helium, neon, xenon, nitrogen, and sulfur hexafluoride (Figs 2–6) show that the multiplication factor $\alpha_i = (1/N_e)\,dN_e/dx$, as it is ordinarily assumed, is proportional to the density (pressure) of the gas and can be written in the form $\alpha_i(E,p) = p\xi(E/p)$, where $\xi(E/p)$ is a function typical for the given gas. For helium and xenon, the following approximation based on the experimental data is known [8, 47]:

$$\xi\left(\frac{E}{p}\right) = A \exp\left[-B\left(\frac{p}{E}\right)^{1/2}\right], \qquad (6)$$

where $A = 4.4$ cm^{-1} Torr^{-1} and $B = 14$ V cm$^{-1/2}$ Torr$^{-1/2}$ for helium, while $A = 65.3$ cm^{-1} Torr^{-1} and $B = 36.1$ V cm$^{-1/2}$ Torr$^{-1/2}$ for xenon.

However, the calculations have shown (see Figs 2 and 6) that this approximation holds only if the reduced electric field strength does not exceed a certain value: $E/p < (E/p)_{max}$; for helium, $(E/p)_{max} = 200$ V cm^{-1} Torr^{-1}, and for xenon $(E/p)_{max} = 1500$ V cm^{-1} Torr^{-1}. At higher values of E/p, the multiplication factor α_i begins to decrease. The drop in α_i with increasing E/p is related to the decrease in the ionization cross section at high energies.

In this connection, Tkachev and Yakovlenko [16, 17] proposed an approximation of the Townsend coefficient that describes its decrease:

$$\xi\left(\frac{E}{p}\right) = A \exp\left[-B\left(\frac{p}{E}\right)^{1/2} - C\,\frac{E}{p}\right], \qquad (7)$$

where $A = 5.4$ cm^{-1} Torr^{-1}, $B = 14$ V cm$^{-1/2}$ Torr$^{-1/2}$, and $C = 0.0017$ cm Torr V^{-1} for helium; $A = 7.2$ cm^{-1} Torr^{-1},

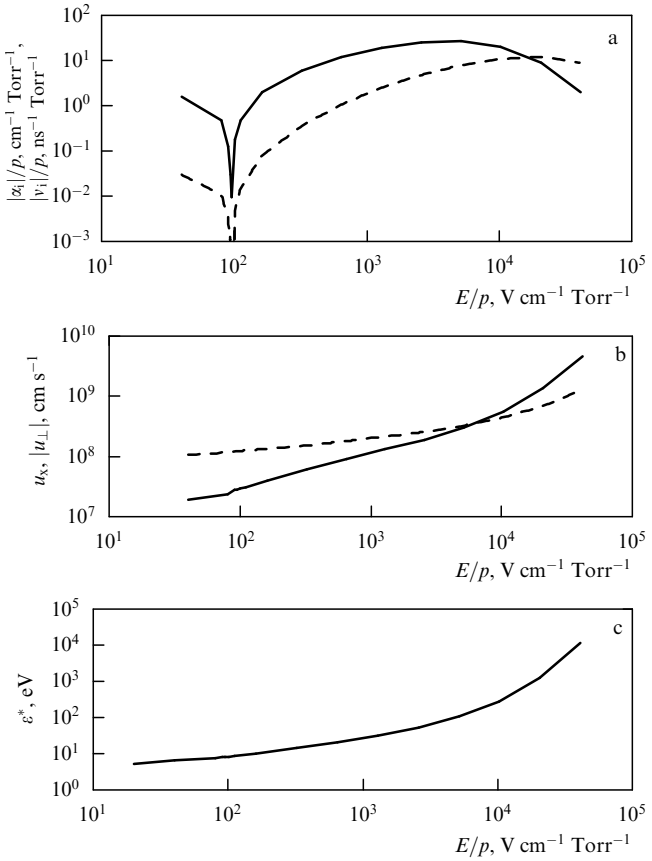

Figure 4. Dependence of the ionization and drift characteristics on the reduced field strength E/p for SF_6. The points were obtained for different electric field strengths at $p = 100$ Torr. (a) Pressure-normalized values of the absolute value of the Townsend coefficient $|\alpha_i|/p$ (solid curve) and of the ionization rate $|\nu_i|/p$ (dashed curve). (b) Mean projection u_x (solid curve) of the electron velocity on the x-axis directed along the electric field, and the mean absolute value of the velocity $|u_\perp|$ (dashed curve) in the plane perpendicular to the x-axis. (c) Mean electron energy.

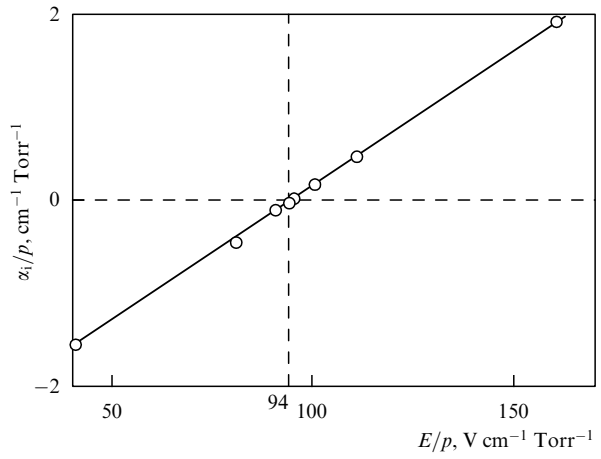

Figure 5. Dependence of the multiplication factor for SF_6 in the transient region. The open circles correspond to the results of calculation, and the solid line represents the linear dependence $2.87 \times 10^{-2} E/p - 2.7$, where the unit of measurement of E/p is 1 V cm^{-1} Torr^{-1}.

$B = 16.1$ V cm$^{-1/2}$ Torr$^{-1/2}$, and $C = 7 \times 10^{-3}$ cm Torr V^{-1} for neon, and $A = 45$ cm^{-1} Torr^{-1}, $B = 31.1$ V cm$^{-1/2}$ Torr$^{-1/2}$, and $C = 1.7$ cm Torr V^{-1} for xenon.

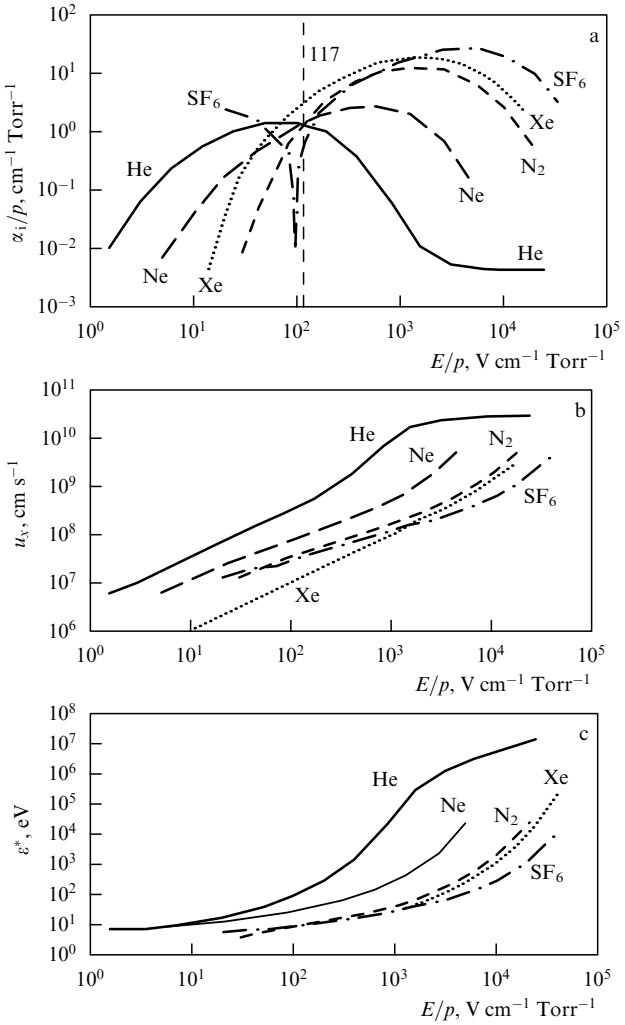

Figure 6. Dependence of the ionization and drift characteristics on the reduced field strength E/p for He, Ne, Xe, N_2, and SF_6. (a) Pressure-normalized values of the Townsend coefficient α_i/p. (b) Mean projection u_x of the electron velocity on the x-axis directed along the electric field. (c) Mean electron energy. In calculating the helium characteristics, relativistic effects were taken into account.

In the case of molecular nitrogen, the following approximation [8, 47] based on the experimental data is used:

$$\zeta_\xi\left(\frac{E}{p}\right) = A \exp\left(-B\,\frac{p}{E}\right), \tag{8}$$

where $A = 12$ cm^{-1} Torr^{-1} and $B = 342$ V cm^{-1} Torr^{-1} for $E/p = 100-600$ V cm^{-1} Torr^{-1}, while $A = 8.8$ cm^{-1} Torr^{-1} and $B = 275$ V cm^{-1} Torr^{-1} for $E/p = 27-200$ V cm^{-1} Torr^{-1}.

The calculations for nitrogen yielded $(E/p)_{\max} = 1500$ V cm^{-1} Torr^{-1} (see Fig. 3).

Note that the value of the peak field strength $E_{\max}$ agrees rather well with the estimate of E_{cr1} done in Section 2.1.1, especially if one takes into account the rough nature of formula (2). Actually, the value of E_{cr1} determines not the condition for continuous acceleration of the majority of electrons with increasing x but is the condition for the drop in the Townsend multiplication coefficient for $E > E_{cr1}$. In this sense, the above values of $E_{\max}$ are simply the more accurate values of E_{cr1}.

2.2.3 The Townsend coefficient in an electronegative gas. It is interesting to examine the mechanism of electron multiplication in an electronegative gas, i.e., a gas with a large cross section of electron attachment to the molecules. In view of the competition between electron attachment and multiplication, it is not clear from the start to what extent the concept of a Townsend coefficient can be applied to an electronegative gas. At the same time, electronegative gases are widely employed in various discharges, in particular, in pumping exciplex and chemical lasers. Boichenko et al. [18] examined electron multiplication and runaway in SF_6, since for this gas the characteristics of electron – molecule collisions are best known.

Calculations have shown (see Figs 4 and 6) that for high values of the reduced electric field strength, $E/p > 94$ V cm^{-1} Torr^{-1}, and large enough electrode spacing, $d > \alpha_i^{-1}$, the Townsend ionization mode is indeed in operation. Qualitatively, the main characteristics of this mode appear to be the same as in the cases of helium, neon, xenon, and nitrogen (see Figs 2, 3, and 6). The function $\xi(E/p)$ has its maximum at $(E/p)_{max} \approx 5$ kV cm^{-1} Torr^{-1}.

An essential feature of an electronegative gas is that in an electric field whose strength is lower than a certain value ($E/p < 94$ V cm^{-1} Torr^{-1} for SF_6) the electrons emitted by the cathode do not multiply; instead, they largely attach to the molecules. The attachment mode that sets in is, in a certain sense, opposite to the multiplication mode, but, like the multiplication mode, is characterized by an exponential dependence for the electron current and the number of inelastic collision acts. At the same time, the mean electron energy ε^* and the velocities u_x and $u_\perp$ are independent of x. However, the multiplication factor is negative in this mode (the Townsend coefficient proves to be negative).

Electron attachment is predominant in electric fields $E/p < 94$ V cm^{-1} Torr^{-1} in which the mean electron energy $\varepsilon^* < 10$ eV becomes much lower than the first ionization threshold (20 eV) of the gas. Within the sign-changing region, the multiplication factor is a linear function of the reduced field strength (see Fig. 5).

Note that according to the experimental data available (see Ref. [8]), the breakdown of SF_6 occurs for $E/p > 117$ V cm^{-1} Torr^{-1}, when $\xi(E/p) > 0$ (see Fig. 6). In their experiments, Panchenko et al. [48] found that at $E/p \approx 117$ V cm^{-1} Torr^{-1} volume discharge in SF_6 also ceases to develop.

2.2.4 Runaway of electrons at relativistic velocities. Since generators in which megavolt voltages are reached in one nanosecond can be devised, it is only proper to ask whether the concept of the Townsend coefficient works at relativistic velocities of the electrons. Helium was taken as an example.[2] When relativistic effects were taken into account (see Fig. 6), after the curve representing the dependence of the Townsend coefficient α_i on E/p had passed its maximum at $E/p \approx 263$ kV cm^{-1} Torr^{-1}, it dropped off very rapidly, but because there is a limitation on the mean electron velocity it becomes almost flat, and then slowly begins to slope upward. This happens at $E/p \approx 6.6$ MV cm^{-1} Torr^{-1}, when $\varepsilon^* \approx 0.5$ MeV, and $u_x \approx 2.3 \times 10^{10}$ cm s^{-1}.

[2] The calculations with allowance for relativistic effects were done by A N Tkachev and S I Yakovlenko.

2.3 Nonlocal electron runaway criterion

2.3.1 Critical voltage. The Townsend ionization mode sets in at a certain distance $x \sim \alpha_i^{-1}$ from the cathode, which corresponds to the characteristic multiplication length. If the electrode spacing is small, $d < \alpha_i^{-1}$, the electron multiplication pattern differs dramatically from the Townsend one (for details see Ref. [16]). A substantial fraction of the electrons is accelerated steadily: as the distance x from the cathode increases, both the x-component of the electron velocity and the mean electron energy ε^* grow. In this case, the peak in the energy distribution function of the electrons that reached the anode occurs at the maximum value of the energy $eU = eEd$ acquired by the electrons in their flight from the cathode to the anode.

In Refs [16–19], in contrast to the traditional approach [6–8], it was assumed that runaway electrodes begin to dominate when the distance d between the electrodes becomes comparable to the characteristic multiplication length, i.e., to the reciprocal Townsend coefficient α_i^{-1}. For $\alpha_i d < 1$, the runaway electrons are also predominant in the energy spectrum of the electrons that have reached the anode. Accordingly, the criterion determining the limiting value E_{cr} of the electric field strength has the form

$$\alpha_i(E_{cr}, p)d = 1\,.$$

In the Townsend coefficient we isolate as a factor the pressure or gas density and employ the fact that the second cofactor is a function only of the reduced electric field strength E/p, i.e., we write $\alpha_i(E,p) = p\,\xi(E/p)$. For flat electrodes, $E = U/d$, with $E_{cr} = U_{cr}/d$. Then, the criterion of electron escape from the gap between the two flat electrodes becomes

$$pd\,\xi\left(\frac{E_{cr}}{p}\right) = 1 \quad \text{or} \quad pd\,\xi\left(\frac{U_{cr}}{pd}\right) = 1\,. \tag{9}$$

This expression presents an implicit dependence of the critical voltage $U_{cr}(pd)$ on the product pd of the pressure and the electrode spacing (Figs 7 and 8). The curve $U_{cr}(pd)$ separates the region of effective electron multiplication from the region in which the electrons leave the discharge gap before they have any time to multiply, and is a universal curve for the given gas. We will call it the electron escape curve.

Note that the value of E_{cr}/p depends on pd, in contrast to E_{cr1}/p which is determined by the local criterion and depends only on the characteristics of the neutral particles. Hence, by their very nature, these quantities are distinctly different: $E_{cr1}/p \approx (E/p)_{max}$, as noted in Section 2.2, corresponds to the peak in the Townsend coefficient, while E_{cr}/p determines the electron escape criterion.

2.3.2 The lower and upper branches of the escape curve. The presence of a maximum in the $\xi(E/p)$ function determines the horseshoe shape of the function $U_{cr}(pd)$ for a broad spectrum of gases (see Fig. 7). Note that, mathematically speaking, it would be more convenient to swap the horizontal pd-axis and the vertical U_{cr}-axis, i.e., to think of pd as a function of U_{cr}. However, we will not do this here, so as not to depart from the tradition related to Paschen curves (see Section 2.4).

The electron escape curve $U_{cr}(pd)$ has two branches: the upper and the lower. We assume that the boundary point between these two branches is the turning point, i.e., the point where pd reaches it minimum value $(pd)_{min}$. We will

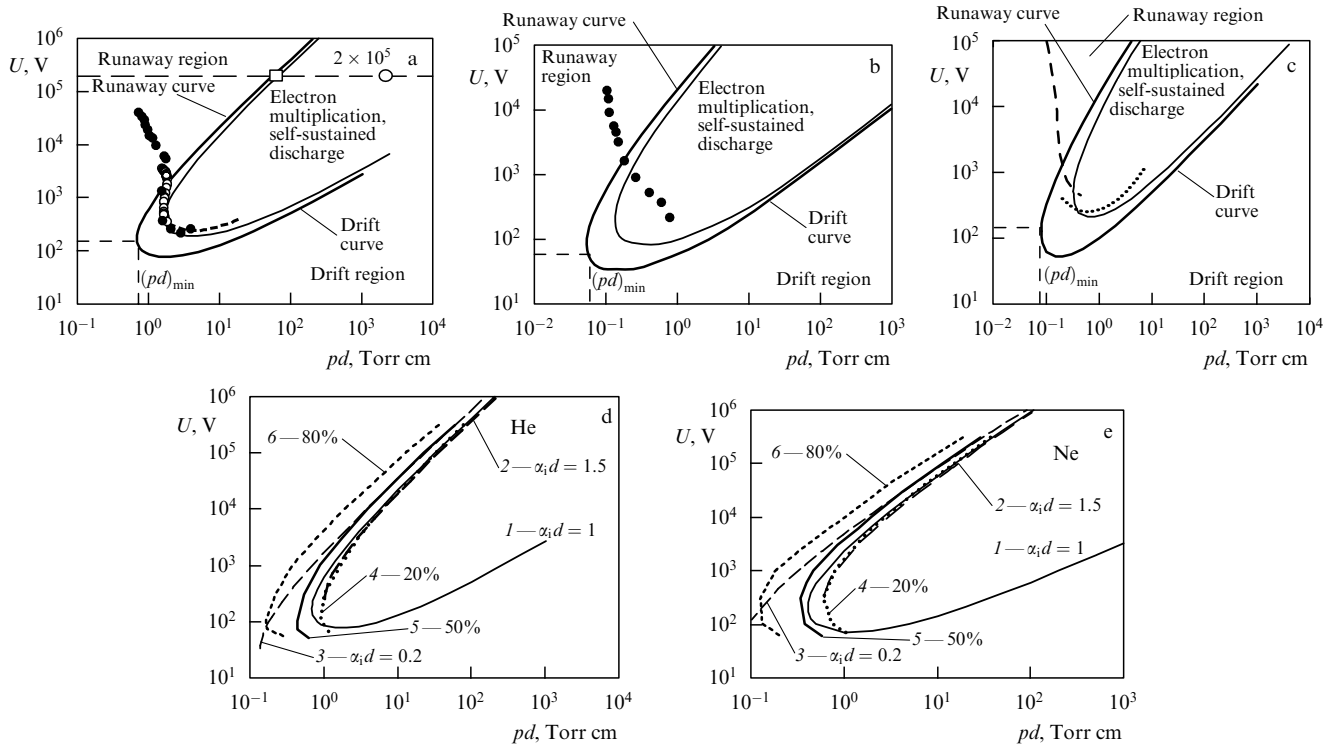

Figure 7. Universal curves characterizing the escape, runaway, and multiplication of electrons. Curves $U_{cr}(pd)$ separate the electron escape and multiplication regions (heavy solid curves) for helium (a), xenon (b), and nitrogen (c); curves $U_{ign}(pd)$ characterizing the discharge ignition criterion (light solid curves) as well as equal efficiency curves and runaway curves for helium (d) and neon (e). In figures a and b, the black circles represent the results of Dikidzhi and Klyarfel'd's experiments [51], and for the $U_{ign}(pd)$ curves it is assumed that $L = \ln(1 + 1/\gamma) = 2.45$. In figure a, the dashed curve represents the experimental data from Ref. [8], and the open circles represent the results of Penning's experiments [50]. The large open circle in the upper right corner of figure a corresponds to the maximum value of the voltage in the experiments described in Ref. [24], which were conducted at atmospheric pressure and a distance $d = 28$ mm between the electrodes, while the large open square corresponds to a situation in which the 'plasma cathode' is at a smaller distance $d = 0.7$ mm from the anode. In figure c, it is assumed that $L = \ln(1 + 1/\gamma) = 4.0$ for the curve $U_{ign}(pd)$; the dotted curve represents the experimental data from Ref. [8], and the dashed curve represents the results of the calculations done by Campbell et al. [40]. In figures d and e: *1*, the runaway curves at $\alpha_i d = 1$; *2*, the runaway curves at $\alpha_i d = 1.5$; *3*, the runaway curves at $\alpha_i d = 0.2$, and *4–6*, the efficiency curves at $\eta = 20$, 50, and 80%, respectively. The efficiency η is defined as the fraction of electrons landing on the anode with an energy exceeding two-thirds of the energy acquired by electrons in free motion, namely $\varepsilon > 2eU/3$.

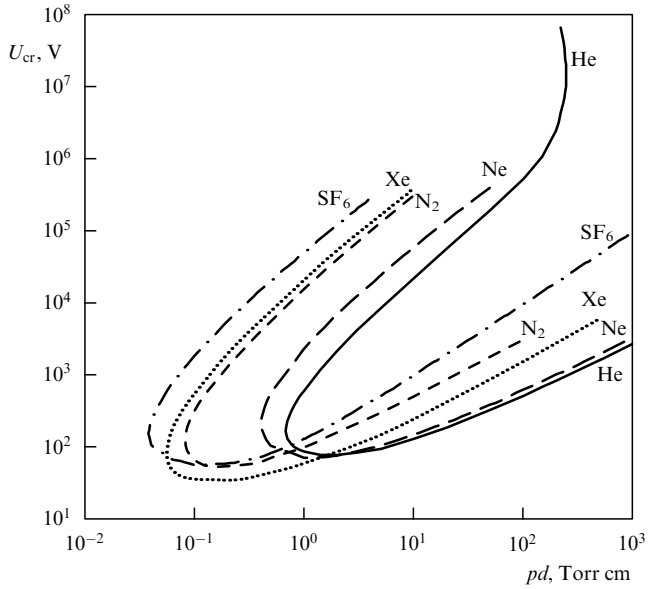

Figure 8. Universal curves $U_{cr}(pd)$ separating the electron escape and multiplication regions for He, Ne, Xe, N_2, and SF_6. In calculating the helium characteristics, relativistic effects were taken into account.

show that this point corresponds to the maximum of the function $\xi(x)$.

Let us think of pd as a function of U_{cr}. For the condition $d(pd)/dU_{cr} = 0$, corresponding to the minimum in the pd vs. U_{cr} dependence, expression (9) yields $\xi'(x) = 0$, which corresponds to the maximum of $\xi(x)$. Thus, the boundary point defined as the minimum value of pd in the $U_{cr}(pd)$ curve corresponds exactly to the value of the reduced field strength $E/p = (E/p)_{max}$ at which the reduced Townsend coefficient $\alpha_i/p = \xi(E/p)$ passes through its maximum.

The existence of an upper branch in the escape curve $U_{cr}(pd)$ is due to the drop in the Townsend coefficient with increasing E/p. In turn, the drop in the Townsend coefficient is caused by the decrease in the ionization cross section as the energy of the incident electrons increases and by the increase in the energy of the electrons being multiplied with a rise in E/p. The region above the upper branch meets the situation in which electrons, while acquiring a large amount of energy on their mean free path, leave the discharge gap without having enough time to effectively multiply because of the small ionization cross sections at high energies. Therefore, it is natural to call the region above the upper branch of the escape curve the electron runaway region (the whistler region), and the upper part of the curve the runaway curve.

The lower branch of the curve corresponds to the increasing part of the dependence of the reduced Townsend coefficient α_i/p on E/p. In this region, the electrons acquire a relatively small amount of energy on their mean free path, and

this amount is appropriate to the increasing part of the dependence of the ionization cross section on the electron energy. The region under the lower curve $U_{cr}(pd)$ fits the situation where the electrons drift from the cathode to the anode and do not acquire enough energy for effective multiplication. Therefore, it is natural to call the region under the lower branch of the escape curve the electron drift region, and the lower part of the curve the drift curve.

If relativistic effects are taken into account, three branches can be identified in the electron escape curve $U_{cr}(pd)$ (see Fig. 8). The appearance of one more turning point in the runaway curve and, hence, of an additional third branch (compared to the nonrelativistic case) is due to the increase in the ionization cross section at high energies as a consequence of relativistic effects. In contrast to the nonrelativistic case for $pd > 230$ Torr cm, electron multiplication occurs at any voltage across the discharge gap, which exceeds the threshold value determined by the drift curve.

2.3.3 Electron-beam production efficiency curves. The definition of the runaway curve implies that it qualitatively characterizes the fraction of runaway electrons. Generally speaking, there is a certain arbitrariness in the choice of the right-hand sides of expressions (9). The right-hand side of Eqn (9) can be set equal not to unity but, say, to π or $1/\pi$. However, it is clear that this choice is not of vital importance. Assuming, for instance, that $\alpha_i d = A = \text{const}$, we get for the new quantity U'_{cr} the equation $pd\,\xi(U'_{cr}/pd) = A$. This leads to a simple relationship between these quantities: $U_{cr}(pd) = U'_{cr}(pd/A)/A$. On the log–log scale, the curve $U'_{cr}(pd)$ can be obtained from the curve $U_{cr}(pd)$ by a simple shift along the coordinate axes.

Although the escape curve qualitatively characterizes the boundary separating the regions of electron multiplication and runaway of electrons, it does directly determine the fraction of the runaway electrons. To establish the quantitative characteristics, calculations of the fraction η of runaway electrons as functions of U and pd were done directly. Here, the efficiency was defined as the fraction of electrons arriving at the anode with an energy exceeding two-thirds of the energy that the electrons would acquire in free motion, namely $\varepsilon > 2eU/3$. The results of these calculations are presented in the form of equal-efficiency curves in the (U, pd)-plane (Figs 7d and e).

These calculations showed that for low enough efficiencies, $\eta \leqslant 20\%$, the runaway curves practically coincide with the equal-efficiency curves. At higher efficiencies, the runaway curves were found to coincide with the equal-efficiency curves only at large values of U and pd.

2.4 On the ignition criterion of a self-sustained discharge

2.4.1 The upper branch of the self-sustained discharge ignition curve. The curve that determines the discharge ignition criterion is usually found from the requirement that each electron must create a sufficient number of ions, so that one more electron is produced at the cathode by secondary electron emission. Accordingly, the discharge ignition potential $U_{ign}(pd)$ is determined by the following condition (e.g., see Ref. [8]):

$$\alpha_i(E,p)d = \ln\left(1+\frac{1}{\gamma}\right) \quad \text{or} \quad pd\,\xi\left(\frac{U_{ign}}{pd}\right) = L\,, \tag{10}$$

where $L \equiv \ln(1+1/\gamma)$, with γ being the secondary electron emission coefficient.

Comparing the expressions for the discharge ignition criteria (10) and for the electron runaway criteria (9), we arrive at a relationship between the escape and ignition curves: $U_{ign}(pd) = L\,U_{cr}(pd/L)$. This relationship was used when constructing the curves $U_{ign}(pd)$ in Fig. 7.

Compared to the well-known Paschen ignition curve, the resulting dependence $U_{ign}(pd)$ carries entirely new information. As is well known, the Paschen curves have right and left branches that extend from the minimum in $U_{ign}(pd)$ to the regions of large and small values of pd. However, according to Refs [16–19], the self-sustained discharge ignition curve is to contain in addition an upper branch resulting from the drop in α_i when E/p increases. An important consequence of the above reasoning is also the presence of a minimum value of $(pd)_{min}$ at which ignition of a self-sustained discharge is still possible due to electron multiplication as a result of gas ionization in the discharge gap.

Notice that Kolbychev [49] pointed out the possibility of the discharge disruption at high voltages.

2.4.2 Comparison with experiments at low pressures. It must be noted, however, that the nature of the ignition curve $U_{ign}(pd)$ is not as general as that of the escape curve $U_{cr}(pd)$. The escape curve $U_{cr}(pd)$ represents a universal characteristic of the given gas, while the ignition curve $U_{ign}(pd)$ depends on the model describing the discharge ignition, in particular, on the properties of the electrodes. For instance, the upper branch is masked by electrode phenomena and can be observed only in open discharges or for very short pulses. This becomes obvious if we compare the results of our calculations with the experimental data for ordinary cathodes (see Fig. 7).

Away back in 1932, Penning [50] showed that the Paschen curve for helium has a loop with a turning point at $pd \approx 1.5$ Torr cm (Fig. 7a). This turning point agrees well with the results of the calculations by Tkachev and Yakovlenko [16], described in Section 2.4.1. Penning rightly assumed that this loop reflects the presence of a maximum in the electron-energy dependence of the ionization cross section. However, his viewpoint did not receive broad support. The reason, probably, was that no such loop was detected in other inert gases (e.g., see Ref. [51]), although the ionization cross sections of all elements possess a maximum. Apart from helium, only in mercury was such a loop observed [52].

Keep in mind that the portion of the Paschen curve that is to the left of the point $(pd)_{min}$ reflects another mechanism of discharge ignition, a mechanism only slightly related to electron multiplication in the gas. This conclusion is supported by the fact that the Paschen curves in this region depend not only on the cathode material but also on the anode material [51]. The mechanism describing the left branch of the Paschen curves for helium was studied by Ul'yanov and Chulkov [53]. They found that the three-valued nature of the curve $U_{ign}(pd)$ in the region around $(pd)_{min}$ is caused by competition between different mechanisms of electron production within the discharge volume and at the electrodes, namely, Townsend ionization, secondary electron emission from the cathode triggered by fast ions and atoms that form as a result of ion charge exchange, and the electron scattering from the anode.

The results of experiments with gases at atmospheric pressure are discussed in Sections 3.1 and 4.1. Modern nanosecond techniques have made it possible to 'get through' the lower branch of the Paschen curve and land

near the runaway curve before the gas-discharge plasma has time to completely short-circuit the interelectrode gap.

3. Electron-beam production in dense gases

3.1 Experiments on electron-beam production in dense gases

3.1.1 History of the problem. Stankevich and Kalinin [54] and Noggle et al. [55] were the first to detect X-ray radiation at atmospheric pressure (in air [54], and in helium [55]). This suggested the presence of accelerated electrons. The discovery of accelerated electrons at atmospheric pressure provided new impetus to the study of the conditions in which such electrons are produced and X-ray radiation is formed in gas-filled diodes at elevated pressures (see the review [6] and references cited therein). However, up to quite recently the amplitude values of the electron-beam currents generated in molecular gases at atmospheric pressure did not exceed fractions of an ampere [6]. In 2002, Alekseev et al. [20–22] found that the amplitude of the electron beam generated in a gas-filled diode at atmospheric pressure can be substantially increased. The experiments involved molecular gases (air and nitrogen), CO_2-N_2-He mixtures, and helium.

High-current electron beams have been generated at mean values of the parameter E/p higher than the critical value, $E/p \gg E_{cr1}/p$ [21], and much lower than the critical value, $E/p \ll E_{cr1}/p$ [20–23]. The latter result required some explanation. To this end, in order to explain the production of electron beams at $E/p \ll E_{cr1}/p$, it was assumed (see Refs [20, 22, 23]) that as the plasma formed near the cathode has a motion toward the anode, the electric field along the discharge gap undergoes a redistribution, and in the part of the gap between the plasma and the foil the field strength becomes higher than E_{cr1}. In other words, in studying the mechanism of beam production in Refs [20, 22, 23], the researchers compared the mean values of E/p attained in the experiments with the critical values E_{cr1}/p that had been calculated by Korolev and Mesyats [7] on the basis of the traditional local electron runaway criterion (see Section 2.1). After issuing Tkachev and Yakovlenko's paper [16], the parameter E_{cr}/p determined by the nonlocal criterion (9) was adopted as the critical field [24]. Accordingly, it was assumed that the main current pulse emerges when the value of the parameter E/p approaches E_{cr}/p, and the point in the (U, pd)-plane the runaway curve (see Section 3.2).

We begin by presenting the results of experiments [20–25] in which the production of an electron beam in a gas-filled diode occurs in a mode in which the maximum amplitudes of the beam current are attained in the region behind the anode.

3.1.2 Experimental facility and methods. The research involved using three generators of nanosecond pulses with capacity energy storages (of the SINUS and RADAN brands), which are described in detail in Refs [56–58], and a fourth generator with inductive energy storage [59]. Schematic diagram of the experimental facility based on the first three generators is shown in Fig. 9. The first pulse generator, which has been described in detail in Ref. [56], generated in a 30-Ω matched load a $\sim$ 200-kV pulse with a half-height duration of roughly 3 ns and a voltage pulse front of roughly 1 ns. This voltage pulse was fed to cathode *2*, while the pressure in the gas gap varied from 10^{-2} to 760 Torr.

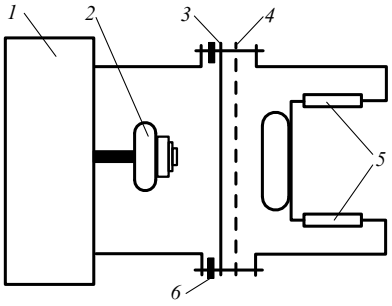

Figure 9. Schematic of the experimental facility [22]: *1*, generator; *2*, cathode; *3*, foil or grid; *4*, additional foil for measuring the electron beam energy; *5*, shunt for measuring the beam current, and *6*, shunt for measuring the total current in the gas-filled diode.

Two different types of cathodes were utilized. The first was a set of three cylinders (12, 22, and 30 mm in diameter) made from 50-μm thick Ti foil. The cylinders were inserted into each other and attached to a duralumin base 36 mm in diameter. All three cylinders had a common axis. The height of the cylinders reduced by 2 mm from the cylinder with the smaller diameter to that with the larger one. The second cathode was made from graphite in the form of a tablet 29 mm in diameter with rounded edges, and the convex side of the tablet with a 10-cm radius of curvature was positioned in front of the foil. The graphite cathode was attached to a copper holder 30 mm in diameter. The beam was extracted through the 45-μm AlBe foil *3*. The gas gap could be varied from 10 to 28 mm.

The second generator (RADAN-303) had a wave impedance of 45 Ω and generated in a matched load the voltage pulses in the 50–170 kV range (with an open-circuit voltage up to 340 kV) with a half-height duration of roughly 5 ns and a voltage pulse front of about 1 ns [57]. The voltage across the gas gap could be continuously varied by changing the gap of the main discharger.

The third generator (RADAN-220) had a wave impedance of 20 Ω and generated in the discharge gap a voltage pulse with an amplitude up to 220 kV and with a half-height duration of roughly 2 ns and a voltage pulse front of about 0.3 ns [58]. The research involved studying a flat anode and a small-sized cathode (as in most works devoted to the study of X-ray radiation and fast electrons in gas-filled diodes), which made possible additional enhancement of the electric field at the cathode. The gas-filled diodes for both RADAN generators had the same design and were similar to those used in Refs [20, 22–25]. The cathode was fabricated from a steel tube 6 mm in diameter and 50 μm in wall thickness, which was attached to a metal rod of the same diameter, or from a graphite rod 6 mm in diameter with rounded or sharp ends. The flat anode (through which the electron beam was extracted) was fabricated from 40-μm thick AlBe foil or 10-μm thick Al foil or a grid with a light transparency in the 20–70% range. The cathode–anode spacing could be varied from 13 to 20 mm. In some experiments, the discharge gap was placed in a gas chamber with windows, which made it possible to evacuate and change the composition and pressure of the gases in the discharge gap.

The fourth generator was equipped with inductive energy storage which comprised the current interrupter based on semiconducting opening switch (SOS) diodes connected in parallel to the load [59, 60]. It generated in the discharge gap

voltage pulses with an amplitude of roughly 50 kV and with a half-height duration of about 15 ns and a voltage pulse front of 7 – 15 ns. Two types of discharge gaps were used with this generator. The anode was fabricated from foil and was flat, while the cathode had a small radius of curvature and was fabricated from 50-μm thick steel foil and had the shape of a tube 6 mm in diameter or a blade 8 cm long with rounded edges. The cathode – anode spacing could be varied between 8 and 30 mm.

To record the signals from the capacitive divider, Faraday cylinders, and shunts, the researchers used a TDS-684B oscilloscope with a 1-GHz bandwidth (5 dots per nanosecond) or a TDS-334 oscilloscope with a 0.3-GHz bandwidth (2.5 dots per nanosecond). The discharge glow was photographed by a digital camera. The integrated signal of the discharge emission was recorded with a vacuum FEK-22 photodiode, whose output signal was fed to the TDS-334 oscilloscope.

3.1.3 Results of measurements. The main experimental findings are given in the following. As shown in Refs [20 – 25], in a nonuniform electric field, with a small-sized cathode and a short voltage front, the discharge mode in the discharge gap is such that in the gas-filled diode an electron beam with a current amplitude amounting to dozens or even hundreds of amperes is produced under atmospheric pressure. The electron beam appears at the front of the voltage pulse and has a ~ 0.3-ns current-pulse half-height duration (Fig. 10a) or can be even shorter. The beam current amplitude at an air pressure of 1 atm in the diode may be as high as 35 A when the beam is extracted through the 40-μm thick AlBe foil for the second generator, and 75 A for the third. The beam current amplitude becomes higher when air is replaced with helium. For helium at atmospheric pressure, the electron beam current beyond the AlBe foil, obtained with the second generator in optimal conditions, was higher than 200 A.

As the voltage amplitude increases, the maximum in the beam current shifts toward the beginning of the voltage pulse, and for maximum voltages ends at the pulse front (Fig. 10b). As the voltage drops, the time lag of the electron beam increases to roughly 1 ns, and the beam is recorded at the beginning of the quasi-stationary phase of the voltage pulse. In this case, the beam current amplitude is drastically reduced. Analysis of the oscillograms of the beam current beyond the foil, conducted under variations in foil thickness, shows that as the foil gets thicker, the maximum in the beam current shifts toward the beginning of the voltage pulse. With a 10-μm thick foil, the maximum in the beam current was recorded after the first maximum in the voltage pulse, and for a foil of maximum thickness, the maximum in the beam current shifts toward the first maximum in the voltage oscillogram.

If the electrode spacing, the length of the voltage pulse front, the type of gas, and the gas pressure (in the given case, this is air at 1 atm) are fixed, there exists only a fairly narrow range of optimal values of the open-circuit voltages of the generator, within which the maximum amplitudes of the electron beam current beyond the foil are observed (Fig. 11). The amplitude of the beam current after the foil with the second generator attained its maximum at a voltage of about 210 kV. However, in these conditions the amplitudes of the pulse voltage across the discharge gap and of the discharge current are practically linear functions of the amplitude of the open-circuit voltage of the second

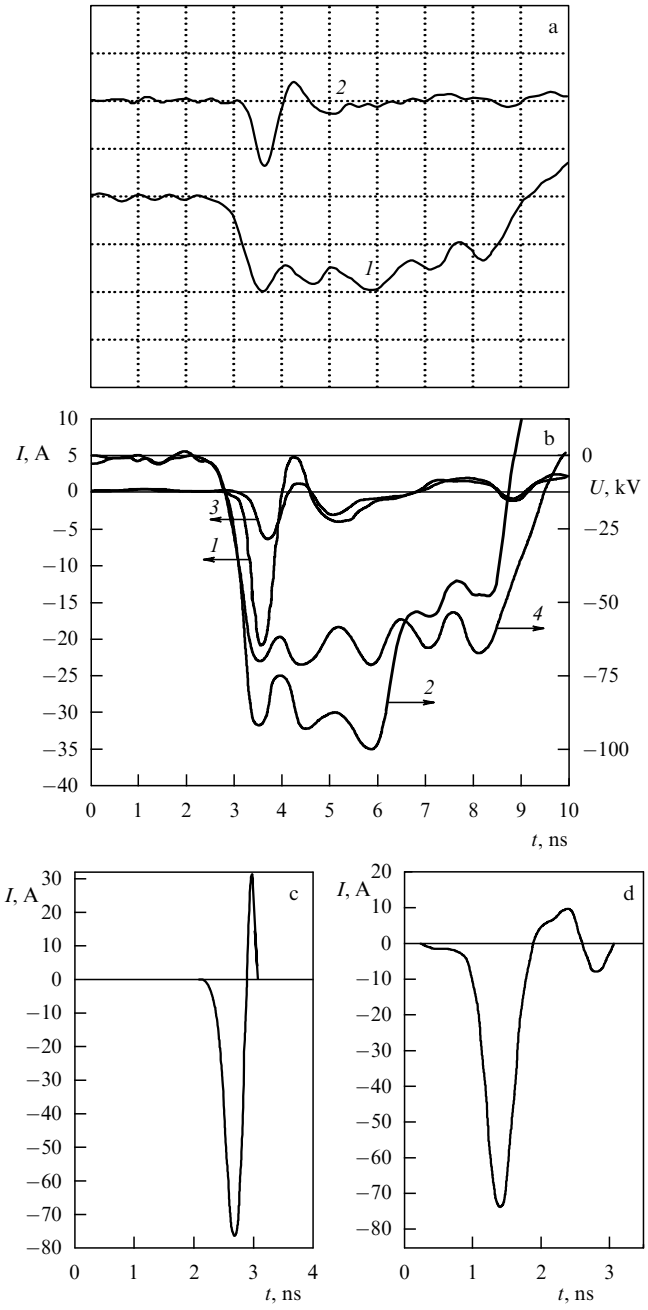

Figure 10. (a) Oscillograms of the voltage across the gas-filled diode (curve *1*) and of the electron beam current (curve *2*) [23]; the horizontal axis is marked in 1 ns per cell, and the vertical axis is marked in 27 A and 1 kV per cell. (b) Oscillograms of the current pulses (curves *1* and *3*) in the electron beam beyond the 40-μm thick AlBe foil and of voltage pulses (curves *2* and *4*) on the gas-filled diode, obtained with the second generator in air at atmospheric pressure. The gap in the diode is $d = 16$ mm, and the open-circuit voltages are 260 kV (curves *1* and *2*) and 155 kV (curves *3* and *4*). (c, d) Oscillograms of the current pulses in the electron beam beyond the 40-μm thick AlBe foil, obtained with the third generator. The gap in the diode is $d = 16$ mm, and collector diameters in figures c and d are 20 and 50 mm, respectively. (Taken from Ref. [24]).

generator (see curves *2* and *3* in Fig. 11). We comment on this result in Section 4.3. Note that the voltage amplitude of the third generator was about 220 kV, which satisfies the optimal conditions for generating a beam current in a gas-filled diode (see Fig. 11). Here, the wave impedance of the second generator was half the wave impedance of the first

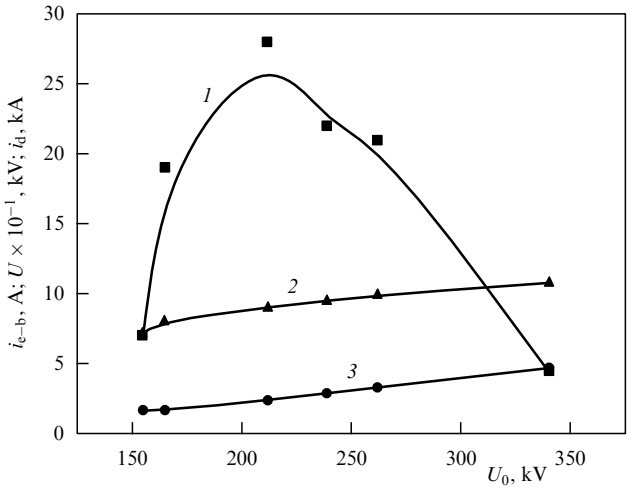

Figure 11. Dependences of the electron beam current beyond the 40-μm thick AlBe foil (*1*), the voltage across the discharge gap (*2*), and the discharge current (*3*) on the open-circuit voltage of the second generator. (Taken from Ref. [24].)

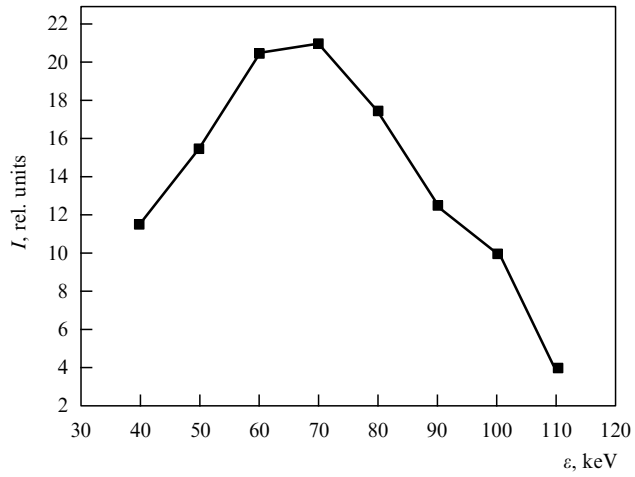

Figure 12. Energy distribution of the beam electrons at an air pressure of 1 atm in the gas-filled diode. The distribution was recorded by the foil method with a 270-kV open-circuit voltage for the first generator. The gap in the diode was $d = 17$ mm. (Taken from Refs [20, 25].)

generator, while the beam current beyond the foil for the second generator was, as we noted earlier, twice as high as that for the first generator. A two-fold increase in the beam current amplitude can be attributed to a two-fold decrease in the wave impedance.

The electrons in the beam in the optimum mode for the air-filled diode have a mean energy that amounts to approximately 60% of the energy corresponding to the maximum voltage across the discharge gap (for the second generator, the mean energy was about 65 keV). A typical energy distribution of the electrons of a beam produced is depicted in Fig. 12. Clearly, the distribution possesses a large half-width. The half-height of this distribution corresponds to electron energies from 40 to 100 keV, i.e., the electrons in a beam are produced at different voltages across the discharge gap. Similar dependences of the current amplitudes on the open-circuit voltage of the second generator were obtained when the foil was replaced by a grid, with the beam current

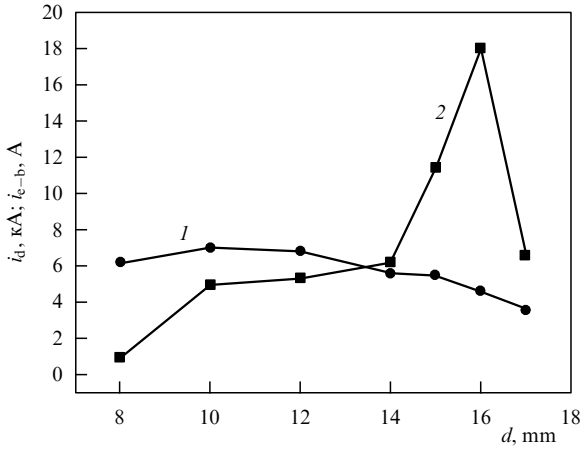

Figure 13. Dependence of the discharge current amplitude (*1*) and the beam current beyond the 40-μm thick AlBe foil (*2*) on the cathode–anode separation (the third generator, cathode of the first type, and the air pressure of 1 atm). The time resolution of the recording system was 1 ns.

amplitude being usually found to decrease with a fall in grid transparency.

Studies on the effect of the magnitude of the electrode spacing on the beam current in air, carried out with the second and third generators in the case of a cathode in the form of a steel tube, have shown that the reduction of gap size down to 16–17 mm leads to a decrease in the beam current beyond the foil. The same effect showed itself when the gap was widened to 18 mm. For a gap wider than 18 mm, partial breakdown to the metal side wall of the diode was observed in the gas-filled diode of the second and third generators. The dependence of the beam current amplitude in air on the gap size, obtained at accelerator *3* (see Fig. 9), is plotted in Fig. 13. Clearly, the maximum amplitude of the discharge current is at a gap size of 16 mm.

Important information may be drawn from the oscillogram of the current pulse (Fig. 10c), which was recorded with a small-sized collector and the highest possible time resolution of the recording system. First, the length of the beam current pulse does not exceed 0.3 ns, when the highest possible time resolution is applied in recording the oscillogram. Second, the time it takes for the beam current amplitude to fall off is in the subnanosecond range. Thus, after the beam current reaches its maximum, the conditions needed for the production of an electron beam in the gas-filled diode deteriorate very rapidly, although the voltage across the diode has not changed significantly.

Figure 14a displays photographs of the discharge glow in air, the end view taken through a grid with 50% transparency, and another view at an angle. The discharge was of the volume type, and bright spots were visible only at the cathode. The photographs in Fig. 14b (side view) show that in the discharge gap there is a glow in the form of diffusion jets with an overall diameter at the anode of no less than 12 mm. The diameter of the luminous spot on the luminescent screen, which is formed by the electron beam produced with the third generator in air at a pressure of 1 atm at a distance of 1 cm from the foil, reached 4 cm.

Thus, the maximum current amplitudes of a beam produced in a gas-filled diode are attained at a subnanosecond front of the voltage pulse, certain voltages of the generator, and a volume discharge in the form of 'jets'.

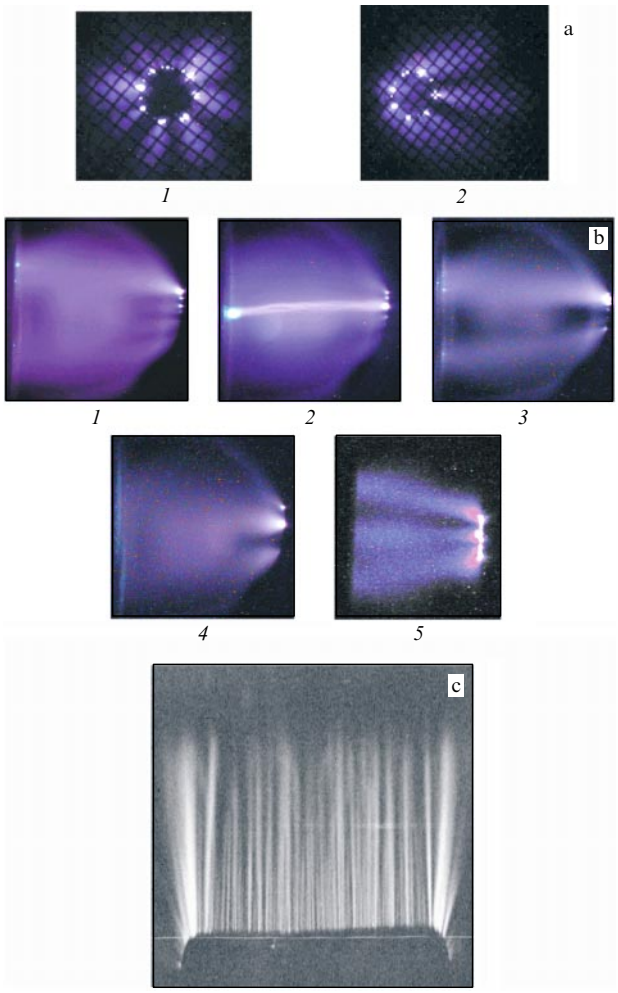

Figure 14. Photographs of the discharge glow: (a) end view (*1*) and picture taken at some angle (*2*), third generator, grid cell size is 1 × 1 mm (taken from Ref. [24]); (b) in argon (*1* and *2*), krypton (*3* and *4*), and air (*5*), side view, photographs *1*, *3*, and *5* were taken at a gas pressure of 1 atm, and photographs *2* and *4* were taken at gas pressures of 0.75 and 0.25 atm, respectively, third generator, electrode spacing is 16 mm; (c) with a foil anode and a blade cathode, $d = 30$ mm, fourth generator (taken from Ref. [59]).

3.2 On the mechanism of electron-beam production at atmospheric pressure

As noted earlier, in interpreting the results of the above experiments, we based our reasoning on the nonlocal criterion (9) for the appearance of a large number of electrons that leave the volume without multiplication [16, 17]. Strictly speaking, this criterion was formulated for flat electrodes. The features associated with the plasma inhomogeneity will be examined in Section 4.2.

We distinguish between two phases in the mechanism of electron-beam production accompanying gas breakdown at atmospheric pressure: the phase in which a volume discharge is created, and the phase of generation of an electron beam proper, which follows the first phase. In general terms, the situation is as follows. Plasma is already created at the front of the voltage pulse, and this plasma short-circuits the discharge gap in the course of roughly a nanosecond. It is this plasma that is the source of the electrons in the beam. By coming nearer to the anode, such a plasma cathode 'shortens' the distance d between the electrodes [61, 62]. As a result, we have conditions close to those for the runaway curve (see Section 2.3), even if at the beginning of the movement toward the anode the plasma parameters corresponded to the region of Townsend electron multiplication.

For instance, if we assume that $d = 28$ mm and $U = 200$ kV for the experiments described in Refs [21, 24], then at $p = 1$ atm we get $pd = 2 \times 10^3$ Torr cm. In Fig. 7a, the respective point in the (U, pd)-plane is marked by a large open circle in the upper right corner. Clearly, for the electron runaway criterion to be met, the value of pd must be smaller than the experimental value by a factor of approximately 30. The electron runaway criterion may be met at instants of time when the plasma traveling from the cathode has moved closer to the anode: at $U = 200$ kV this happens when $pd = 55$ Torr cm, which means the criterion is met, for instance, at $d = 0.7$ mm (in Fig. 7a, this point is marked by a large open square).

The discharge production stage in a gas-filled diode is discussed below in Section 4.2.

4. Production of a nanosecond discharge at atmospheric pressure

4.1 Experiments on volume-discharge production at atmospheric pressure without a supplementary preionization source

The usual approach to creating a volume discharge in atomic and molecular gases and their mixtures at elevated pressures is to preionize the discharge gap by using various sources of ionizing radiation [7]. The plasma of such a discharge is widely used in pulsed dense-gas lasers [63]. There is also another way to produce a diffusive discharge without preionizing the gas at atmospheric pressure in a nonuniform electric field with nanosecond excitation pulses [6]. In this case, short voltage pulses with a steep edge (from several nanoseconds to fractions of a nanosecond) are applied to the discharge gap. However, the reasons why, and the conditions in which, a volume discharge forms in a nonuniform nanosecond electric field have not been studied, and the input power density has not exceeded 100 MW cm^{-3}. In this section we examine the results of studies concerning volume-discharge formation in a nonuniform electric field with voltage pulses of nanosecond duration [23, 24, 59].

The nanosecond-pulse generators used in the experiments were those described in Section 3.1. Volume discharges were ignited in air, nitrogen, helium, neon, argon, and krypton.

The following facts were established from measurements of the voltage pulses across the gas-filled diode and the discharge current and from observations of the shape of the discharge in the discharge gap. Within a broad range of experimental conditions and for all the investigated gases, between the tube cathode with a sharp-pointed edge and the anode there emerges a volume discharge in the form of diffusion cones or 'jets' (see Fig. 14). The discharge remains diffusive at different pressures, and only at the cathode are there bright spots which appear at the front of the voltage pulse. Note that the volume discharge can be obtained in conditions corresponding to the production of an intense electron beam with electron energies in the dozens and hundreds of kiloelectron-volts (see Section 3.1) as well as in conditions where no electron beam is detected beyond the foil.

As the interelectrode gap is made smaller or the design of the cathode is changed or pressure is varied, individual

channels may be observed against the background of the diffusive discharge (see photograph *2* in Fig. 14b), while in nonoptimal conditions (e.g., small gap) the discharge may transform into the spark stage. As the generator voltage increases (in optimal conditions for the gap), against the background of the volume discharge there also appear brighter filamentary channels, and a drop in voltage is registered on the voltage oscillogram (oscillogram *2* in Fig. 10b). Figures 14a and b display photographs of discharge glow in air, taken from a side view in the case of a foil anode, and in end and slant views in the case of a grid anode. As noted earlier, the discharge appears in the form of volume jets which originate from the bright spots at the cathode. For a blade-shaped cathode, the discharge also appears in the form of diffusion jets (see Fig. 14c).

The discharge current is recorded with a very small time lag (fractions of a nanosecond) in relation to the instant of time the voltage is applied to the discharge gap. The size and duration of the discharge current in a volume discharge depend on the generator parameters, the interelectrode gap, and the type and pressure of gas. For instance, for the first generator with an open-circuit voltage of roughly 270 kV, the discharge current amplitude amounted to about 2400 A. When the volume nature of the discharge remained such for 3 ns, with the first generator the current density at the anode reached 3 kA cm^{-2}, the specific energy deposited to the gas amounted to 1 J cm^{-3}, and the input power density was more than 400 MW cm^{-3}. When the volume stage was maintained for 5 ns, the current density at the anode reached 1.5 kA cm^{-2}, the input power density was roughly 200 MW cm^{-3}, and the specific energy deposited to the gas reached again ~ 1 J cm^{-3}. In the given experiment, the discharge was maintained in the self-sustained regime, in which the voltage across the discharge gap is at its maximum in the quasi-stationary discharge stage, i.e., the electron concentration at the front of the voltage pulse in the discharge gap is high. Note that, usually, when the voltage pulse applied to the discharge gap has a steep edge, there appears an overvoltage peak, even if UV or X-ray preionization has been used, and only then does the quasi-stationary discharge stage set in [63, 64].

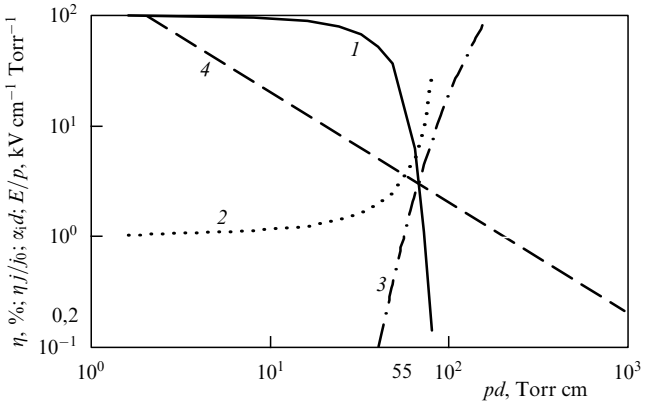

Figure 15. Dependence of the current characteristics on the product of the pressure by the length of the discharge gap for helium. Curve *1* represents the fraction η (in percentage point) of beam electrons, related to the total number of the electrons that reached the anode; curve *2* exhibits the current of the runaway electrons produced by a single electron, $\eta j/j_0$ (j_0 is the current from the cathode, and j is the current at the anode); curve *3* represents the parameter characterizing the runaway of electrons, $\alpha_i(E,p)d$, at $E = 125$ kV cm^{-1}, and curve *4* exhibits the reduced electric field strength E/p. The beam electrons are assumed those with the energy $\varepsilon > 2eU/3; d = 16\,\text{mm}, U = 200\,\text{kV}; E = 200/16\,\text{kV mm}^{-1} = 125\,\text{kV cm}^{-1}$.

4.2 On preionization mechanisms

4.2.1 Fast electrons. Let us discuss in detail the first phase, i.e., the formation mechanism of plasma that approaches the anode. As noted earlier, a nanosecond discharge at atmospheric pressure appears diffusive in photographs, i.e., it contains no spark channels (see Fig. 14). Only near the cathode are there small bright regions of plasma glow. It is well known that a volume discharge at atmospheric pressure is formed even in the pulsed mode, provided there has been effective preionization. It is only natural to assume that such preionization is available by fast electrons.

In this connection, it would be interesting to follow the changes in the various characteristics of the electron beam being produced in the range of *pd* values fitting the electron runaway curve. The range of values represented in Fig. 15 corresponds to the straight line $U = \text{const}$ (see Fig. 7a) connecting the points marked by an open square and a large open circle.

As one would expect, the fraction of fast electrons begins to drop rapidly (see Fig. 15, curve *1*) at *pd* values such that for a given value of U the magnitude of $\alpha_i d = pd\,\xi(U/pd)$, which characterizes runaway of electrons, becomes comparable to unity (curve *3*). The sharp bend in curves *1* and *2* corresponds to the vicinity of the point $pd \approx 55$ Torr cm, where $pd\,\xi(U/pd) \approx 1$.

Note that within the range of parameters represented in Fig. 15, the magnitude of E/p everywhere exceeds $(E/p)_{\max} = 0.2$ kV cm^{-1} $Torr^{-1}$, at which value the Townsend coefficient begins to decrease and, according to the notion adopted, runaway of the majority of electrons will occur. However, it is seen from Figs 7 and 8 that the electron runaway mode is implemented only at small *pd* values. This is an additional argument in favor of the substantial difference in the criteria $E/p = (E/p)_{\max} = E_{cr1}/p$ and $\alpha_i(E_{cr}, p)d = 1$ discussed in Sections 2.1 and 2.3.

What may seem somewhat unexpected is that despite the drop in the number the electrons in the beam at $U_{cr}(pd) > U$ their current near the same point $pd \approx 55$ Torr cm increases dramatically (curve *2*). This is quite natural, however. With the number of ionization acts on the rise, the number of fast electrons must also increase. Here, of course, as *pd* grows, there is an ever increasing number of low-energy electrons, compared to the number of runaway electrons. Hence, the fraction of runaway electrons drops. The rise in the electron beam current beyond the anode with increasing p, as well as with increasing d, has been verified in experiments [21].

In view of the multiplication of runaway electrons, it can be expected that they are the cause of strong preionization at relatively low voltages, $U < U_{cr}(pd)$. Here, the plasma inhomogeneity may be of importance.

4.2.2 Field concentration. It is natural to relate the mechanism of plasma formation in the volume between the cathode and the anode to the appearance of fast electrons emitted by the above-mentioned small plasma protuberances at the cathode. Fast kilovolt electrons ensure preionization of the gas between the cathode and the anode. Hence, the discharge at atmospheric pressure is relatively uniform. The production of fast electrons near a tip is related to the field concentration at the ends of the conducting plasma protuberances near the cathode.

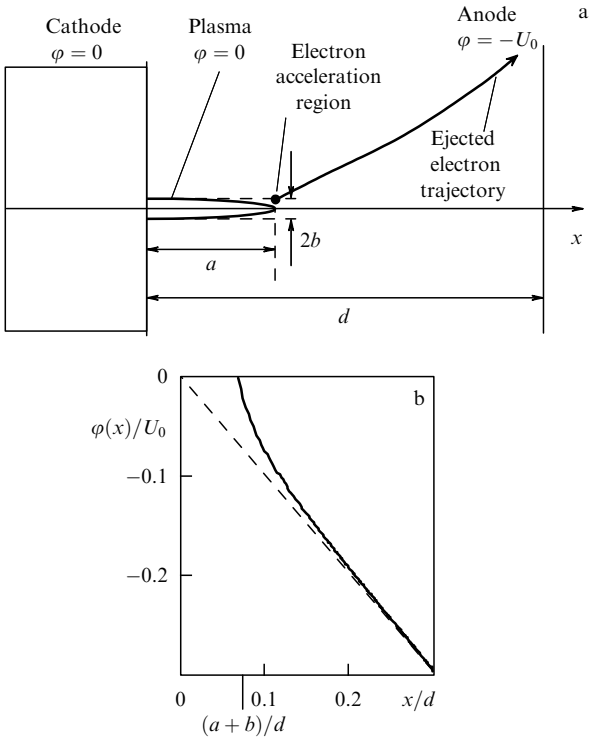

Figure 16. Geometry of the problem (a) and the distribution of potential (b) along the x-axis, which is the continuation of the major axis of the ellipsoid and is measured from the flat surface of the cathode. The parameter values used in the calculations are $d = 28$ mm, $a = 1$ mm, and $b = 0.5$ mm.

To clarify this point, we examine the results of the well-known electrostatic problem on the distribution of the electric field potential, when the cathode has a conducting asperity in the form of one-half of an elongated ellipsoid of revolution, whose axis is perpendicular to the planes of the plates [65] (Fig. 16a). The distribution of the potential is given by the formula

$$\varphi(\xi,\zeta) = -\frac{U_0}{d}\, x(\xi,\zeta)\left\{1 - \left[\ln\left(\frac{1+\varepsilon}{1-\varepsilon}\right) - 2\varepsilon\right]^{-1} \times \left[\ln\left(\frac{\sqrt{1+\xi/a^2}+\varepsilon}{\sqrt{1-\xi/a^2}-\varepsilon}\right) - \frac{2\varepsilon}{\sqrt{1+\xi/a^2}}\right]\right\},$$

where ξ and ζ are the parabolic coordinates, U_0 is the potential difference between the flat electrodes, $x(\xi,\zeta) = (a/\varepsilon)\sqrt{(1+\xi/a^2)(1+\zeta/a^2)}$ is the coordinate along the field direction, a and b are the major and minor semiaxes of the ellipsoid, respectively, and $\varepsilon = \left[1-(b/a)^2\right]^{1/2}$ is the eccentricity of the ellipsoid. This solution is valid if $d - a \gg b$.

We can draw the following conclusion from the exact solution (Fig. 16b). As expected, the voltage drop near a tip occurs over a distance on the order of the tip's radius of curvature ($\sim b$). However, the magnitude of this drop is not determined by the tip's curvature but by the distance a from the tip's end to the cathode: $\varphi(a+b) = -U_0(a+b)/d$. Indeed, turning the radius of the field curvature to zero, we get an infinitely large field strength but a finite drop in the potential: $\varphi(a) = -U_0 a/d$. The magnitude of this drop is determined by how far from the cathode the end of the inhomogeneity tip is. Of course, these general conclusions about the size of the region of potential drop and on the magnitude of the potential drop are valid not only in the case of an elliptic protuberance but also for a 'needle' of any shape.

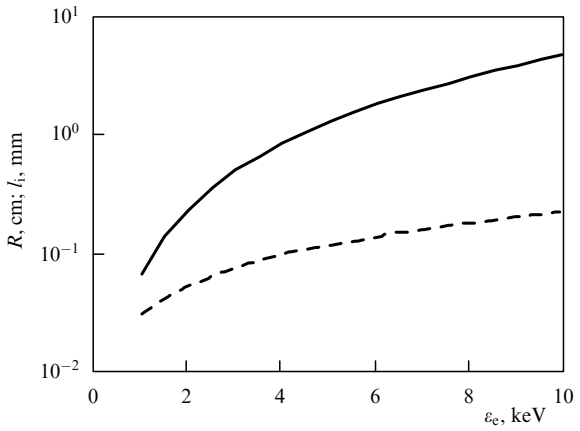

Figure 17. Dependence of the free path R (solid curve) and of the distance l_i between the places of ionization acts (dashed curve) on the electron energy ε_e. The approximation adopted in Ref. [16] was used for $\sigma_i(\varepsilon_e)$.

Here are some estimates. From the photographs in Fig. 14 it follows that the size of the bright regions near the cathode's surface is approximately 1 mm. We assume that electron number density in the cathode spot is high and that the protuberance is a good conductor. We also assume that the conductivity of the plasma surrounding the protuberance is moderate. In such conditions, the distribution of the potential that forms is close to the one considered in the model electrostatic problem.

The electrons that have been emitted by the tip and have travelled a distance $\sim (2-3)b$ acquire an energy $\varepsilon_e \approx eU_0 a/d$. The energy of the fast electrons 0.5 – 1 ns after the voltage pulse has been applied to the discharge gap, with the peak $U_0 \approx 100$ kV, will amount to roughly 1 – 4 keV. The free path of these electrons, $R = (\varepsilon_e/\varepsilon_i) l_i$, increases in proportion to the square of ε_e (Fig. 17) and amounts to $R \sim 0.1-1$ cm at $\varepsilon_e \sim 1-4$ keV. Here, $\varepsilon_i = 46$ eV is the energy spent on a single ionization act (the energy of formation of an ion pair), $l_i = 1/\sigma_i N \sim 0.1$ mm is the free path of the electron in a time from one ionization act to another, $\sigma_i(\varepsilon_e)$ is the ionization cross section, and $N \approx 2.4 \times 10^{19}$ cm^{-3} is the helium density.

4.2.3 On the preionization by accelerated electrons. Let us take a qualitative look at the possible role that externally injected accelerated electrons play in the formation of an ionization wave [66]. When an electron is injected into the gas with a sufficiently high velocity, it becomes accelerated steadily. According to Fig. 1, for instance, for an injected 1-keV electron to become accelerated at all times at atmospheric pressure, an electric field strength of 25 kV cm^{-1} is sufficient, and this is much lower than the peak field strength in experiments in which electron beams are produced (see Section 3.1). Moving in the medium, this electron leaves behind a trace of electrons produced. And it is these secondary electrons that form avalanches.[3] Accordingly, for the spatial – temporal distribution of the number of electrons produced by a fast electron we have the result

$$n_e = \exp\left\{\nu_i\left[t - \tau(x)\right]\right\},$$

[3] The shape of a solitary electron avalanche in helium has been examined by Tkachev and Yakovlenko [67].

where $\nu_i = \alpha_i u_d$ is the rate of ionization in the avalanche, u_d is the avalanche's propagation velocity, and $\tau(x)$ is the time that it takes the electron to travel from the cathode ($x = 0$) to the point x in question. To calculate the electron number density distribution on the basis of n_e, the latter must be multiplied by the number density of ionization acts along the electron's path and the path density. Calculations of the path density require a separate study.

Ignoring the friction force for fast electrons and assuming that they move along the field, we get

$$n_e(\nu_i t, \alpha_i x) = \exp\left[\nu_i t - b\left(\sqrt{1 + a\alpha_i x} - 1\right)\right],$$

$$\nu_i \tau(x) = b\left(\sqrt{1 + a\alpha_i x} - 1\right),$$

where

$$a = 2\,\frac{eE}{m_e}\,\frac{1}{\alpha_i v_0^2}, \qquad b = \frac{m_e}{eE}\,\alpha_i v_0 u_d,$$

with v_0 being the initial velocity of the externally injected electron, and E the external electric field strength.

An ionization wave is generated when the avalanche build-up time $1/\nu_i$ begins to exceed the time $\tau_d = \tau(d)$ it takes the fast electrons to travel the length of the discharge gap, i.e., when $\nu_i t_d < 1$. At higher ionization rates, the electron number density behind the fast electron rapidly grows. If the ionization rate is low, the entire discharge gap becomes ionized simultaneously since a uniform seed ionization is provided, with no ionization wave being generated.

When electron multiplication is rapid, the plasma layer in the region extending from the cathode to a point $x_{cr} < x_e$ (x_e is the coordinate of the fast electron) screens the external electric field, and the cathode appears to close in on the anode. This screening occurs in a sizable part of the volume when, due to avalanche multiplication, the electron number density reaches the value of $N_{e,cr} = U_0/4\pi e d^2 \sim 10^{10}$ cm^{-3}. When the ionization wave approaches the anode, $x_{cr} \approx d$, the field strength rapidly increases, while the Townsend coefficient decreases. Then, as noted earlier, in a narrow layer between the plasma formed in the volume and the anode the nonlocal electron runaway criterion (9) is met, and a high-power electron beam is produced.

4.3 Background multiplication front in a nonuniform field

4.3.1 The simplest model. Let us discuss in detail the mechanism for the propagation of ionization, originating in the exponential multiplication of background electrons with a low number density in a nonuniform electric field [68 – 70]. At the points in space where the field strength is higher, the multiplication is more intense, while in regions with a low field strength the multiplication is less intense. The field is concentrated at the cathode spot. Hence, near the cathode's surface the electrons multiply faster. As the electron number density grows, the electric field is screened and the plasma boundary moves on.

To explain the mechanism of the multiplication wave, we take the simplest model possible. We ignore electron drift and determine the boundary between plasma and gas at the points where the plasma density reaches a certain critical value N_{cr} at which the field is completely screened. In this case, the dependence of the electron number density on the radius vector $\mathbf{r}$ of the point in question and on time t is given by the expression

$$N_e(\mathbf{r}, t) = \begin{cases} N_0 \exp\left[\nu_i\big(E(\mathbf{r})\big)t\right] & \text{for } N_0 \exp\left[\nu_i\big(E(\mathbf{r})\big)t\right] < N_{cr}, \\ N_{cr} & \text{for } N_0 \exp\left[\nu_i\big(E(\mathbf{r})\big)t\right] \geqslant N_{cr}, \end{cases} \tag{11}$$

where N_0 is the background plasma density. Clearly, in model (11) the direction in which ionization wave propagates does not depend on the sign of the field's projection onto this direction, since the ionization rate is determined by the absolute value of the electric field strength. Hence, Tkachev and Yakovlenko [67] and Yakovlenko [68, 69] proposed a photonless model of a streamer, based on equation (11).

4.3.2 Velocity of the multiplication front. The coordinates of the multiplication wave front are determined by the points at which the electron number density reaches its critical value. Let us examine the time dependence of the coordinate $z(t)$ of one of the points of the wave front along the normal to the front. Implicitly, $z(t)$ is determined by the expression

$$\nu_i\big(E_0(z(t))\big)t = \mathrm{Ln}, \qquad \mathrm{Ln} \equiv \ln\frac{N_{cr}}{N_0}, \tag{12}$$

where $E_0 = E\big(z(0)\big)$ is the electric field strength at the surface of the front. Generally speaking, both Ln and N_{cr} are functions of E_0. However, we ignore this dependence in view of its logarithmic nature. Taking the time derivative of formula (12), we get

$$u_{fr} = \frac{dz}{dt} = \nu_i\left[\left(\frac{d\ln\nu_i}{d\ln E}\left|\frac{-\nabla E}{E}\right|\right)_{E=E_0}\mathrm{Ln}\right]^{-1}. \tag{13}$$

If we approximate a section of the surface near the wave front by a sphere of radius r_0, then $|-\nabla E/E|_{E=E_0} = 2/r_0$. Accordingly, one has

$$u_{fr} = \nu_i r_0\left[\left(\frac{d\ln\nu_i}{d\ln E}\right)_{E=E_0} 2\mathrm{Ln}\right]^{-1}. \tag{14}$$

The ionization rate $\nu_i = \alpha_i u_{de}$ can be written down as the product of the Townsend coefficient $\alpha_i(E,p) = p\,\xi(E/p)$ by the electron drift velocity $u_{de}(E/p)$. Thus, the velocity of the ionization front is expressed in terms of the functions of E_0/p that are universal for the given gas:

$$u_{fr} = \frac{\nu_i r_0}{\zeta(E_0/p)}, \qquad \zeta\left(\frac{E_0}{p}\right) = 2\,\mathrm{Ln}\left\{\frac{d\ln\big[u_{de}(E/p)\,\xi(E/p)\big]}{d\ln(E/p)}\right\}_{E/p=E_0/p}. \tag{15}$$

4.3.3 Front velocity in helium and xenon. Let us discuss in detail the velocity of the ionization front in helium and xenon, since for these gases the ionization and drift characteristics have been thoroughly described (see Section 2.2). For helium [16], one finds

$$\xi(x) = 5.4\exp\left[-\left(\frac{14}{x}\right)^{1/2} - 1.5\times10^{-3}\,x\right]\ [\mathrm{Torr}^{-1}],$$

$$u_{de} = 10^6 x\ [\mathrm{cm\ s}^{-1}]. \tag{16}$$

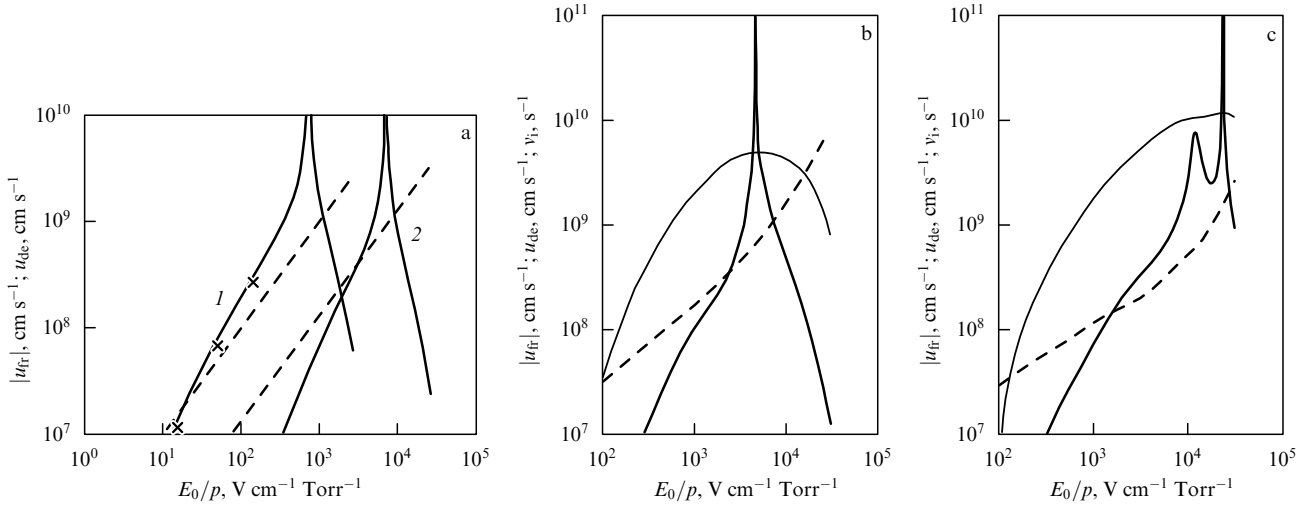

Figure 18. Dependence of the absolute value of the velocity $|u_{fr}|$ (heavy solid curves) of the ionization front, the drift velocity u_{de} (dashed curves), and the ionization rate ν_i (light solid curves) on the reduced field strength E_0/p at the streamer surface: (a) for helium and xenon. The calculations were done by using formulas (16)–(19). The crosses mark the results of numerical treatment on the basis of model (11) (see the main text). Curves *1* correspond to helium, and curves *2* to xenon; (b) for N_2, $(E_0/p)_{cr} \approx 4.7$ kV cm^{-1} Torr^{-1}, and (c) for SF_6, $(E_0/p)_{cr} \approx 23$ kV cm^{-1} Torr^{-1}. In the entire range of the parameters $\alpha_i r_0 > 10$, $N_{cr} = 10^{14}$ cm^{-3}, $N_0 = 10$ cm^{-3}, $r_0 = 0.5$ mm, and $p = 1$ atm.

Substituting formula (16) into expressions (15), we get

$$u_{fr} = \frac{\nu_i r_0}{\zeta(x)}, \quad \zeta(x) = 2\,\mathrm{Ln}\,(1 + 1.87x^{-1/2} - 1.5\times 10^{-3}x)\,. \tag{17}$$

Here, $x = (E_0/p) \times (\mathrm{Torr\ cm\ V^{-1}})$. For helium, one has $(E_0/p)_{cr} \approx 720$ V cm^{-1} Torr^{-1}.

In the case of xenon, the following approximations were used in modeling (see Refs [17, 26]):

$$\xi(x) = 45u_{de}\exp\left[-31.1\left(\frac{1}{x}\right)^{1/2} - 1.7\times 10^{-4}\,x\right]\,[\mathrm{Torr^{-1}}]\,, \tag{18}$$

$$u_{de} = \frac{1.3x + 1.3x^6}{1 + 7.31\times 10^{10}x^{5.8}} + 1.3\times 10^5\,x\exp\left(-\frac{2.2}{x}\right)\,[\mathrm{cm\,s^{-1}}]\,. \tag{19}$$

For xenon, it follows that $(E_0/p)_{cr} \approx 7$ kV cm^{-1} Torr^{-1}. Figure 18 displays the dependence of the wave front velocity in helium and xenon on the reduced electric field strength.

Equation (17) was verified directly by numerical calculations for the case of a spherically symmetric bunch [68–70]. The distribution of the electron number density at different moments in time was calculated by formula (11). The results were then used to calculate the values of the front radius r_{fr} at different moments in time, which were approximated by a linear dependence determining the wave front velocity. Several points obtained in this way are shown in Fig. 18a.

4.3.4 Front velocity in N_2 and SF_6. To analyze the velocity of the background multiplication front in N_2 and SF_6 (Fig. 18b, c), we used the quantities α_i and u_{de} tabulated in Refs [19, 18], respectively. The nonmonotonic character of the velocity of the background multiplication front in SF_6 can be related to the nonmonotonic nature of the derivative of the ionization rate. This nonmonotonicity is caused by the fact that SF_6 possesses three threshold values of the ionization energy (20, 40, and 50 eV).

4.3.5 Simulating the multiplication wave. According to the experimental data, ionization of the discharge gap occurs in the form of 'jets', so to say. Such a jet can be qualitatively represented as a sector of a circle in cylindrical geometry [71]. Hence, to establish the mechanisms of the breakdown of the interelectrode gap, we used a one-dimensional diffusion–drift model described in detail in Ref. [62]. This model describes the development of ionization between coaxial cylindrical electrodes with $r_0 < r < r_1$, where r_0 and r_1 are the radii of the inner and outer electrodes, respectively. The processes of plasma formation and electric-field screening were described by the equations of momentum transfer and continuity for the electrons and ions, as well as the Poisson equation for the electric field. The dependences of the various quantities present in the equations of the drift-dissipative model (ionization rates, drift velocities, and diffusion coefficients) on the field strength were specified by the approximations obtained in Ref. [26].

Calculations have shown that in the case of almost flat electrodes $(d = r_1 - r_0 \ll r_1)$ propagation of the ionization wave is possible only at low voltages and, accordingly, at small Townsend multiplication factors α_i $(\alpha_i d < 1)$. The ionization wave propagating from the cathode to the anode in the case of almost flat electrodes was produced only when there was initially a region of excessive ionization near the cathode. Notice that near the cathode we indeed saw bright plasma formations (see Fig. 14) in all discharge regimes. The condition needed for an ionization wave to be generated meets a situation in which the electrons leave the discharge gap without having time to essentially multiply. In the opposite case $(\alpha_i d \gg 1)$, volume ionization occurs faster than the electron drift, so that the wave does not have enough time to propagate significantly during ionization.

When the electrodes are coaxial cylinders and the cathode has a small radius $(d = r_1 - r_0 \gg r_0)$, the ionization wave forms both at low and high voltages. It propagates not because of electron drift but because of the nonuniformity of the electric field. At the points where the field is stronger, the ionization is more intense. In this case, the plasma density

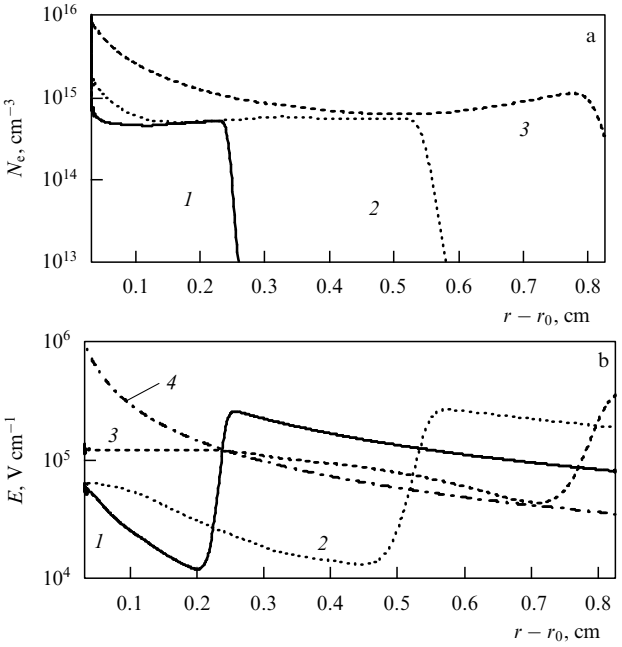

Figure 19. Radial distributions of the electron number density (a) and the electric field strength (b) at moments in time when the ionization wave approaches the anode. The curves correspond to different moments in time: *1*, 1.3 ns; *2*, 1.4 ns, and *3*, 1.5 ns. Curve *4* fits the field distribution $E(r) = -[U/\ln(r_0/r_1)]/r$ in empty space, at $U = 100$ kV, $r_0 = 0.25$ mm, and $r_1 = 8$ mm. The time dependence of the voltage fixed across the electrodes corresponds to the one depicted in Fig. 15.

grows faster to values at which the field is screened, and all further increase in ionization stops.

Figure 19 shows an ionization wave in a nonuniform field. Note that the wave of elevated plasma density is preceded by the wave of elevated electric field strength in the near-anode region. A similar calculation was then carried out for the same conditions, but the voltage $U(t)$ at the instants of time $t > 1$ ns was increased two-fold. Qualitatively, the results agree with those shown in Fig. 19 for lower voltages. Despite an increase in voltage, the electric field strength in the near-anode region at the instant of time when the ionization wave approaches that region does not increase significantly. However, the time it took the ionization wave to cover the distance to the anode decreased.

4.3.6 On the optimal voltage. The results of calculations make it possible to interpret the beam production mechanism in the following manner. According to the discussion in Section 3.2, we assume that the beam electrons are formed near the anode in a layer with a thickness of roughly $1/\alpha_i$. This happens at those moments in time when the ionization wave approaches the anode and the electric field strength in this layer increases. But when the ionization wave touches the anode, the field strength in the near-anode region drops dramatically, although the previous voltage across the electrodes is sustained. Clearly, the conditions for beam production in this case deteriorate.

The following must be said about the reasons for this decrease in the beam current (see also Fig. 11). We should probably speak not of a decrease in current but of a decrease in charge transferred by the beam as the peak voltage across the electrodes increased. Indeed, in the experiments discussed here it was impossible to determine current durations shorter than 0.3 ns. Hence, even if the beam current was high but, because of the short duration of the current (< 0.3 ns), the charge transferred by the beam small, then due to the limited time resolution this would appear as a decrease in the beam current. The decrease in the amount of charge transferred by the beam with increasing voltage can be explained by the reduction of the time the ionization wave spends in traveling through the region where the electron beam is produced, i.e., within a layer that is roughly $1/\alpha_i$ thick and is located near the anode. The validity of this qualitative explanation has been corroborated by the above calculated results.

5. Conclusions

In the present review we have capsuled the discussion about recent studies on the physics of discharges in gases at pressures on the order of atmospheric pressure, which are related to the production of high-power subnanosecond electron beams.

Using a simple equation that allows for electron multiplication, we found that at a certain distance from the cathode a specific value of the mean electron energy that is independent of the spatial coordinate sets in, even if the electric field strength is so high that electron friction in the gas can be ignored. This implies that the local electron runaway criterion (i.e., in the whistler mode) is not sufficiently general to include electron multiplication.

We presented the results, which support this viewpoint, of numerical simulations of electron multiplication and transfer of electrons in helium, neon, xenon, nitrogen, and sulfur hexafluoride. We also showed that the Townsend ionization mechanism (characterized by constant velocity and energy of the electrons combined with an exponential increase in the number of electrons) operates even at field strengths at which electron friction can be ignored. What is important is that the electrode spacing be much larger than the multiplication length (the reciprocal Townsend coefficient).

We examined the nonlocal electron runaway criterion, according to which a large number of electrons in the interelectrode gap are runaway electrons when the electrode spacing becomes comparable to the reciprocal Townsend coefficient. The nonlocal criterion differs very significantly from the local criterion used today. In particular, different recommendations for electron beam production in gases follow from the criteria.

The nonlocal criterion leads to a universal (for the given gas) dependence of the critical voltage $U_{cr}(pd)$ across the interelectrode gap (at which the runaway electrons constitute a substantial fraction of the total number of electrons) on the product pd of the gas pressure by the electrode spacing. The curve $U_{cr}(pd)$ separates the region of effective electron multiplication from the region where the electrons leave the discharge gap without having time to multiply. The curve has an upper and lower branch. The upper branch characterizes runaway of electrons, and the lower branch the escape by drift. The minimum value of pd in the curve $U_{cr}(pd)$ corresponds to the maximum in the dependence of the Townsend coefficient on E/p. Calculations of the $U_{cr}(pd)$ curves have been carried out for helium, neon, xenon, nitrogen, and sulfur hexafluoride.

The $U_{cr}(pd)$ curves were used to build analogs of the Paschen curves $U_{ign}(pd)$ which characterize the ignition of a self-sustained discharge. The curves differ from the known Paschen curves in that they have an upper branch. The ideas

developed in the course of the study have been used to explain the results of experiments on the production of high-current subnanosecond beams of runaway electrons.

Electron beams with currents amounting to dozens or even hundreds of amperes have been produced in gas-filled diodes with different gases at atmospheric pressure. The experimental investigations have shown that for achieving a maximum beam current in a gas-filled diode the discharge must be of the volume type, and the increase in the voltage across the discharge gap must be stopped just before the beam current reaches its maximum. The electron beam produced in such gas-filled diodes has been used to initiate a discharge in an atmospheric-pressure carbon dioxide laser [72].

Volume discharges have been studied in a nonuniform electric field as well. The findings suggest that a volume discharge is formed in a nonuniform electric field because of preionization by fast electrons. Fast kilovolt electrons are produced near the cathode, being accelerated in the strong electric field near cathode plasma formations. Here are the parameters of a volume discharge produced without preionization from supplementary sources at elevated pressures: input power density higher than 400 MW cm^{-3}, discharge current density in the near-anode region up to 3 kA cm^{-2}, and specific energy deposition of about 1 J cm^{-3} in the course of 3 – 5 ns. The quasi-stationary stage of a volume discharge is formed at lower initial voltages, which also supports the formation of a large number of fast electrons.

We have made estimates and done model calculations that show that the main pulse of the electron beam is formed at the instant of time when the plasma in the discharge gap closes in on the anode and when the nonlocal electron runaway criterion is met. We studied the possibility that the plasma formations at the cathode emit fast electrons. We also examined the wave of multiplication of a seed preionization of the discharge gap by runaway electrons in a nonuniform electric field, a wave that begins at the cathode spots.

We believe that subnanosecond electron beams produced in gas-filled diodes will find wide application in various fields of physics and technology. It is quite possible that such a method of producing subnanosecond electron beams can compete with the traditional approach [73]. Here are two possible areas of their applications. First, short high-current electron beams are needed in studies of properties of insulators and semiconductors. In solids, the relaxation times of many processes after excitation amount to several fractions of a nanosecond or even shorter; accordingly, this requires using electron beams of small duration with a short fall time. Second, accelerators that employ the simple design of a gas-filled diode can be used in mining precious stones. As is well known, many crystals (e.g., diamonds), when excited by an electron beam, give off luminescent light in the visible part of the spectrum, so that by exciting samples of a previously prepared rock with an electron beam we can discover precious fragments in it [74].

We are grateful to our co-authors in Refs [16 – 26, 59, 66] for making the valuable contribution to the results presented in this review. The work was made possible by the financial support of the International Science and Technology Center (grants 1270 and 2706).

References

1. Giovanelly R G *Philos. Mag.* **40** 206 (1949)
2. Dreicer H *Phys. Rev.* **115** 238 (1959); **117** 329 (1960)
3. Kulsrud R M et al. *Phys. Rev. Lett.* **31** 690 (1973)
4. Gurevich A V *Zh. Eksp. Teor. Fiz.* **39** 1296 (1960) [*Sov. Phys. JETP* **12** 904 (1961)]
5. Marchenko V S, Yakovlenko S I *Fiz. Plazmy* **5** 590 (1979) [*Sov. J. Plasma Phys.* **5** 331 (1979)]
6. Babich L P, Loĭko T V, Tsukerman V A *Usp. Fiz. Nauk* **160** (7) 49 (1990) [*Sov. Phys. Usp.* **33** 521 (1990)]
7. Korolev Yu D, Mesyats G A *Fizika Impul'snogo Proboya Gazov* (Physics of Pulsed Breakdown of Gases) (Moscow: Nauka, 1991)
8. Raĭzer Yu P *Fizika Gazovogo Razryada* (Gas Discharge Physics) 2nd ed. (Moscow: Nauka 1992) [Translated into English (Berlin: Springer-Verlag, 1997)]
9. Bokhan P A, Sorokin A R *Zh. Tekh. Fiz.* **55** (1) 88 (1985) [*Sov. Phys. Tech. Phys.* **30** 50 (1985)]
10. Kolbychev G V, Kolbycheva P D, Ptashnik I V *Zh. Tekh. Fiz.* **66** (2) 59 (1996) [*Tech. Phys.* **41** 144 (1996)]
11. Sorokin A R *Zh. Tekh. Fiz.* **68** (3) 33 (1998) [*Tech. Phys.* **43** 296 (1998)]
12. Sorokin A R *Pis'ma Zh. Tekh. Fiz.* **28** (9) 14 (2002) [*Tech. Phys. Lett.* **28** 361 (2002)]
13. Bokhan P A, Zakrevsky D E *Pis'ma Zh. Tekh. Fiz.* **28** (11) 21 (2002) [*Tech. Phys. Lett.* **28** 454 (2002)]
14. Derzhiev V I et al., in *Plazmennye Lazery Vidimogo i Blizhnego UF Diapazonov* (Plasma Lasers of the Optical and Near-UV Ranges) [Trudy IOFAN (Proc. General Physics Institute), Vol. 21, Ed. S I Yakovlenko] (Moscow: Nauka, 1989) p. 5
15. Yakovlenko S I "Gazovye i plazmennye lazery" ("Gas and plasma lasers"), in *Entsiklopediya Nizkotemperaturnoĭ Plazmy* (Encyclopedia of Low-Temperature Plasma) (Ed. V E Fortov) Introductory Volume IV (Moscow: Nauka, 2000) p. 262
16. Tkachev A N, Yakovlenko S I *Pis'ma Zh. Eksp. Teor. Fiz.* **77** 264 (2003) [*JETP Lett.* **77** 221 (2003)]
17. Tkachev A N, Yakovlenko S I *Pis'ma Zh. Tekh. Fiz.* **29** (16) 54 (2003) [*Tech. Phys. Lett.* **29** 683 (2003)]
18. Boichenko A M, Tkachev A N, Yakovlenko S I *Pis'ma Zh. Eksp. Teor. Fiz.* **78** 1223 (2003) [*JETP Lett.* **78** 709 (2003)]
19. Tkachev A N, Yakovlenko S I *Pis'ma Zh. Tekh. Fiz.* **30** (7) 14 (2004) [*Tech. Phys. Lett.* **30** 265 (2004)]
20. Alekseev S B, Orlovskiĭ V M, Tarasenko V F *Pis'ma Zh. Tekh. Fiz.* **29** (10) 29 (2003) [*Tech. Phys. Lett.* **29** 411 (2003)]
21. Alekseev S B et al. *Pis'ma Zh. Tekh. Fiz.* **29** (16) 45 (2003) [*Tech. Phys. Lett.* **29** 679 (2003)]
22. Alekseev S B et al. *Prib. Tekh. Eksp.* (4) 81 (2003) [*Instrum. Exp. Tech.* **46** 505 (2003)]
23. Tarasenko V F, Orlovskiĭ V M, Shunaĭlov S A *Izv. Vyssh. Uchebn. Zaved. Ser. Fiz.* **46** (3) 94 (2003) [*Russ. Phys. J.* **46** 325 (2003)]
24. Tarasenko V F et al. *Pis'ma Zh. Eksp. Teor. Fiz.* **77** 737 (2003) [*JETP Lett.* **77** 611 (2003)]
25. Tarasenko V F et al. *Pis'ma Zh. Tekh. Fiz.* **29** (21) 1 (2003) [*Tech. Phys. Lett.* **29** 879 (2003)]
26. Tkachev A N, Yakovlenko S I *Proc. SPIE* **4747** 271 (2002); *Laser Phys.* **12** 1022 (2002)
27. Krishnakumar E, Srivastava S K *J. Phys. B: At. Mol. Opt. Phys.* **21** 1055 (1988)
28. Fursa D V, Bray I *Phys. Rev. A* **52** 1279 (1995)
29. Nickel J C et al. *J. Phys. B: At. Mol. Phys.* **18** 125 (1985)
30. Krishnakumar E, Srivastava S K *J. Phys. B: At. Mol. Opt. Phys.* **21** 1055 (1988)
31. Eletskiĭ A V, Smirnov B M *Fizicheskie Protsessy v Gazovykh Lazerakh* (Physical Processes in Gas Lasers) (Moscow: Energoatomizdat, 1985) p. 44, Table 3.4
32. Engelhardt A G, Phelps A V, Risk C G *Phys. Rev.* **135** A1566 (1964)
33. Golden D E *Phys. Rev. Lett.* **17** 847 (1966)
34. Blaauw H J et al. *J. Phys. B: At. Mol. Phys.* **13** 359 (1980)
35. Dalba G et al. *J. Phys. B: At. Mol. Phys.* **13** 4695 (1980)
36. Krishnakumar E, Srivastava S K *J. Phys. B: At. Mol. Opt. Phys.* **23** 1893 (1990)
37. Tian C, Vidal C R *J. Phys. B: At. Mol. Opt. Phys.* **31** 5369 (1998)
38. Rapp D, Englander-Golden P, Briglia D D *J. Chem. Phys.* **42** 4081 (1965)
39. Schram B L et al. *Physica* **31** 94 (1965)
40. Campbell L et al. *J. Phys. B: At. Mol. Opt. Phys.* **34** 1185 (2001)
41. Cartwright D C et al. *Phys. Rev. A* **16** 1041 (1977)

42. Schulz G J *Rev. Mod. Phys.* **45** 423 (1973)
43. Vicic M, Poparic G, Belic D S *J. Phys. B: At. Mol. Opt. Phys.* **29** 1273 (1996)
44. Stanski T, Adamczyk B *Int. J. Mass Spectrom. Ion Phys.* **46** 31 (1983)
45. Novak J P, Fréchette M F *J. Appl. Phys.* **55** 107 (1984)
46. Kline L E et al. *J. Appl. Phys.* **50** 6789 (1979)
47. Ward A L *J. Appl. Phys.* **33** 2789 (1962)
48. Panchenko A N et al. *Kvantovaya Elektron.* **33** 401 (2003) [*Quantum Electron.* **33** 401 (2003)]
49. Kolbychev G V *Zh. Tekh. Fiz.* **52** 511 (1982) [*Sov. Phys. Tech. Phys.* **27** 326 (1982)]
50. Penning F M *Physica* **12** (4) 65 (1932)
51. Dikidzhi A N, Klyarfel'd B N *Zh. Tekh. Fiz.* **25** 1038 (1955)
52. Guseva L G, Klyarfel'd B N *Zh. Tekh. Fiz.* **24** 1169 (1955)
53. Ul'yanov K N, Chulkov V V *Zh. Tekh. Fiz.* **58** 328 (1988) [*Sov. Phys. Tekh. Fiz.* **33** 201 (1988)]
54. Stankevich Yu L, Kalinin V G *Dokl. Akad. Nauk SSSR* **177** 72 (1967)
55. Noggle R C, Krider E P, Wayland J R *J. Appl. Phys.* **39** 4746 (1968)
56. Gubanov V P et al. *Izv. Vyssh. Uchebn. Zaved. Ser. Fiz.* **39** (12) 110 (1996)
57. Yalandin M I, Shpak V G *Prib. Tekh. Eksp.* (3) 5 (2001)
58. Zagulov F Ya *Prib. Tekh. Eksp.* (2) 146 (1989)
59. Tarasenko V F et al. *Izv. Vyssh. Uchebn. Zaved. Ser. Fiz.* **47** (2) 96 (2004)
60. Kostyrya I D, Tarasenko V F *Opt. Atmos. Okeana* **14** 722 (2001)
61. Arnold E et al. *Laser Phys.* **12** 1227 (2002)
62. Tkachev A N, Yakovlenko S I *Laser Phys.* **13** 1345 (2003)
63. Mesyats G A, Osipov V V, Tarasenko V F *Pulsed Gas Lasers* (Bellingham, Wash.: SPIE, Opt. Eng. Press, 1995)
64. Savin V V, Tarasenko V F, Bychkov Yu I *Zh. Tekh. Fiz.* **46** (1) 198 (1976) [*Sov. Phys. Tech. Phys.* **21** 113 (1976)]
65. Batygin V V, Toptygin I N *Sbornik Zadach po Elektrodinamike* (Problems in Electrodynamics) (Moscow: GIFML, 1962) [Translated into English (London: Academic Press, 1964)]
66. Kostyrya I D et al. *Pis'ma Zh. Tekh. Fiz.* **30** (10) 31 (2004) [*Tech. Phys. Lett.* **30** 411 (2004)]
67. Tkachev A N, Yakovlenko S I *Zh. Tekh. Fiz.* **74** (3) 91 (2004) [*Tech. Phys.* **49** 371 (2004)]
68. Yakovlenko S I *Elektron. Zh.* "*Issledovano v Rossii*" (9) 86 (2004); http://zhurnal.ape.relarn.ru/articles/2004/009.pdf
69. Yakovlenko S I *Kratk. Soobshch. Fiz. FIAN* (10) 27 (2003)
70. Yakovlenko S I *Pis'ma Zh. Tekh. Fiz.* **30** (9) 12 (2004) [*Tech. Phys. Lett.* **30** 354 (2004)]
71. Tarasenko V F et al. *Pis'ma Zh. Tekh. Fiz.* **30** (8) 68 (2004) [*Tech. Phys. Lett.* **30** 335 (2004)]
72. Alekseev S B, Orlovskiĭ V M, Tarasenko V F *Kvantovaya Elektron.* **33** 1059 (2003) [*Quantum Electron.* **33** 1059 (2003)]
73. Zheltov K A *Pikosekundnye Sil'notochnye Elektronnye Uskoriteli* (Picosecond High-Current Electron Accelerators) (Moscow: Energoatomizdat, 1991)
74. Bakhteev V V, Osipov V V, Solomonov V I *Geofizika* (6) 37 (1994)